White paper

syngo.MI Neuro Cortical Analysis

Quantification software for amyloid and tau PET imaging

Rachid Fahmi, PhD and Günther Platsch, MD

siemens-healthineers.com/mi

SIEMENS Healthineers

Table of contents

Introduction

Alzheimer's disease (AD) is the most prevalent neurodegenerative disease and the leading cause of dementia. Pathologically, AD is characterized by the deposition of both extracellular amyloid-β (Aβ) plaques and intracellular hyperphosphorylated tau protein. Depositions of these two proteins occur in different regions and at different rates in the aging brain. In AD, it is hypothesized that extracellular accumulation of Aβ plaques is followed by intracellular tau-associated neurofibrillary tangles (NFTs) aggregation, with a possibility of a positive feedback loop whereby tau mediates Aβ toxicity. Together, Aβ and tau pathologies lead to neurodegeneration, and then to cognitive and clinical decline. AD-type tau is synthesized throughout the brain and the rest of the nervous system and is involved in the formation and stabilization of both three and four microtubule-region repeats (3R/4R). Abnormal tau deposition also occurs in other neurodegenerative diseases or 'tauopathies,' which are characterized by the aggregation of different tau species and tau spreading schemes. Such diseases include progressive supranuclear palsy (PSP) and frontotemporal lobar degeneration (FTLD), which are characterized by 4R and 3R tau deposits, respectively.

Both Aβ and tau deposition can be confirmed either at autopsy or measured in-vivo using cerebrospinal fluid (CSF), plasma samples, or positron emission tomography (PET) imaging.

Amyloid PET imaging

The first developed amyloid PET ligand was the Pittsburgh compound B (^{11}C-PiB) followed by the development and approval for clinical use of three fluorinated radiopharmaceuticals (^{18}F-florbetapir, ^{18}F-florbetaben, and ^{18}F-flutemetamol) for adults with memory problems being evaluated for AD or other causes of cognitive decline. Despite their varying kinetics and dynamic ranges, these radiotracers target the same protein aggregate and exhibit similar imaging characteristics with high white matter retention 30 to 50 minutes post injection, primarily due to delayed clearance of the lipophilic compound as well as non-specific binding of tracer to white matter.[1] A typical negative amyloid PET scan shows high contrast in uptake between the gray and white matter with less intense retention in the gray matter compared to the white matter. A positive scan, on the other hand, is also characterized by high tracer uptake in cortical gray matter due to abnormal plaque deposition. Examples of such scans are shown in Figures 1 and 3.

In addition, cerebellar uptake is consistently low for healthy controls, mild cognitive impairment (MCI), and AD patients as confirmed by histopathologic observations. Consequently, the cerebellum is often used as a reference region when quantifying Aβ PET scans using standardized uptake value ratio (SUVr), which refers to the ratio of radiotracer uptake in a target cortical region to that in a reference region. Other reference regions, such as the pons and the cortical white matter, are also used. SUVr-based quantification of Aβ PET is often used as an adjunct to visual read, which is considered to be the gold standard interpretation method. However, accurately characterizing the degree of amyloid deposition in early cases may be difficult with visual estimation. This is due to the complex folds of cerebral grey and white matter, the interlacing between the two, and multiple tortuous indentations of grey matter into white matter, as illustrated on Figure 1.

Quantification can potentially provide additional diagnostic information and support for readers with less experience, and when assessing borderline cases. However, differences between tracer kinetics and image processing pipelines, including how cortical and reference regions are defined, result in SUVr variability. This renders SUVr-based comparisons and makes defining cutoff points across different tracers very challenging. To address this problem, the Centiloid (CL) scaling method[2] was proposed to harmonize amyloid PET measures across different radiotracers and processing pipelines by transforming measures such as SUVr into the common Centiloid scale.

Two large cohort studies demonstrate the clinical significance of amyloid PET: the IDEAS[3] and AMYPAD[4] trials, which showed that using amyloid PET resulted in clinical management change and increased confidence in diagnosis of patients with MCI or dementia.

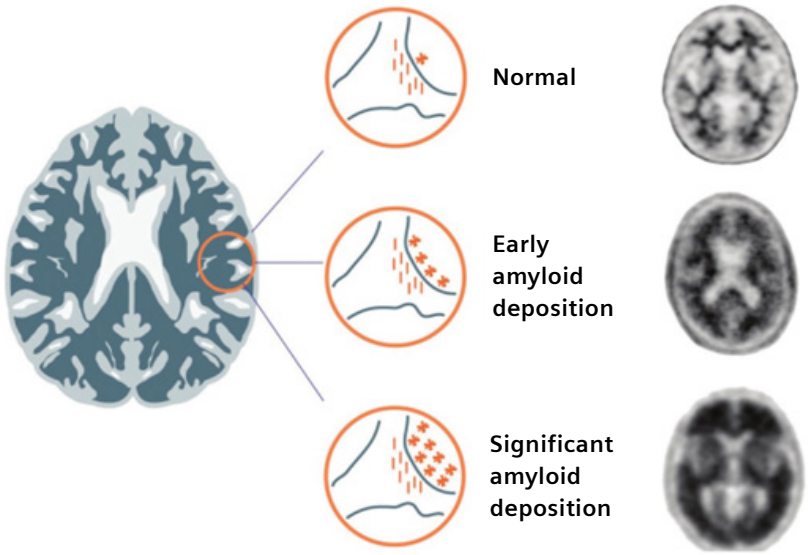

Figure 1. Different amyloid-β deposition patterns in white and gray matter.

Tau PET imaging

Several tau PET ligands have been developed and investigated in the context of AD. These ligands are often categorized into first-generation (e.g., ^{18}F-AV1451, ^{18}F-THK5351, and ^{11}C -PBB3) and second-generation (e.g., ^{18}F-PI2620, ^{18}F-MK6240, ^{18}F-JNJ-311, ^{18}F-GTP, and ^{18}F-RO948) ligands. To date, ^{18}F-flortaucipir, also known as T807 and ^{18}F-AV1451, is the only tau tracer approved for clinical use by the U.S. Food and Drug Administration (FDA).

First- and second-generation tau PET tracers have different binding characteristics and off-target binding (non-tau sites) profiles. For example, ^{18}F-AV1451 and ^{18}F-THK5351 also bind to monoamine oxidase-B (MAO-B) enzymes in the basal ganglia, which could limit their clinical utility in diseases where tau deposition occurs in areas with high MAO-B load.[5] Off-target binding has also been reported in the choroid plexus for ^{18}F-flortaucipir, which often contaminates the signal in the adjacent hippocampus due to partial volume effects.

Second generation tracers, on the other hand, have been shown to have significantly reduced binding in MAO-B rich areas. However, elevated signal in the skull and meninges have been reported for some of these tracers including ^{18}F-RO 948 and ^{18}F-MK6420. Such off-target signals may spill into adjacent cortical areas and must be considered when interpreting tau PET images.

With the advent of tau PET ligands, investigating the role of tau pathology in the onset and progression of other tauopathies, such as the 4R tauopathy movement disorder, PSP, as well as their differential diagnosis, is now possible. For example, tau PET imaging with ^{18}F-PI 2620 was shown to improve the diagnosis of PSP when added to structural magnetic resonance imaging (MRI)[6], making it a potentially valuable biomarker for early diagnosis and drug development.

Unlike Aβ plaques, tau deposition density and distribution have been shown to strongly correlate with brain atrophy and hypometabolism and to closely correlate with concurrent cognitive performance in AD.[7-9] In another study[10], tau PET was shown to be a superior predictor of cognitive decline compared to amyloid PET and MRI. In addition, tau PET imaging, unlike Aβ PET imaging, shows a strong spatial correlation with the clinical and anatomical variability in AD. In Ossenkoppele et al. (2016)[8], it was shown that ^{18}F-flortaucipir uptake was higher in clinically affected posterior regions of the brain in patients with posterior cortical atrophy. In La Joie et al. (2020)[9], the authors reported a strong association between baseline ^{18}F-flortaucipir PET and longitudinal atrophy as measured with MRI, with a notable similarity between the two patterns at the group as well as at the individual level.

Increased accumulation of AD-like tau NFTs in the medial temporal lobe (MTL), as measured by tau PET, has also been shown in older individuals both cognitively impaired and unimpaired, in the absence of amyloid-β pathology. This condition, known as primary aging-related tauopathy (PART), is not yet well understood. In Costoya-Sánchez et al. (2023)[11], individuals with PART exhibited slow progressive tau accumulation that remained restricted to the MTL with no detectable Aβ accumulation, and slow progressive neurodegeneration compared to patients with typical AD.

Stages of tau deposition in Alzheimer's disease

The AD-related tau pathological process spans decades, a time during which deposits of tau NFTs usually follow a regular pattern, spreading from the transentorhinal cortex to the neocortical association areas, and finally to the primary and secondary cortical regions, as demonstrated in a landmark postmortem study by Braak and Braak in 1991,[12] and illustrated on Figure 2. This led to a six-stage tau spreading model known as the Braak staging model.[12-14] Clinically, the first two stages (Braak I-II or the transentorhinal stage) are asymptomatic, the next two stages (Braak III-IV or the limbic stage) correspond to MCI, and the last two stages (Braak V-VI or the neocortical stage) are ultimately associated with dementia. With the recent development of tau PET tracers, several studies have shown that patterns of tau tracer retention correspond well with the topographical NFTs' Braak staging model in AD.[15-18] For instance, Schwartz et al. (2016)[16] demonstrated in-vivo Braak staging using tau PET imaging with ^{18}F-flortaucipir across the AD spectrum (cognitively normal, MCI, and AD dementia) in 86% of the studied cohort (N = 173).

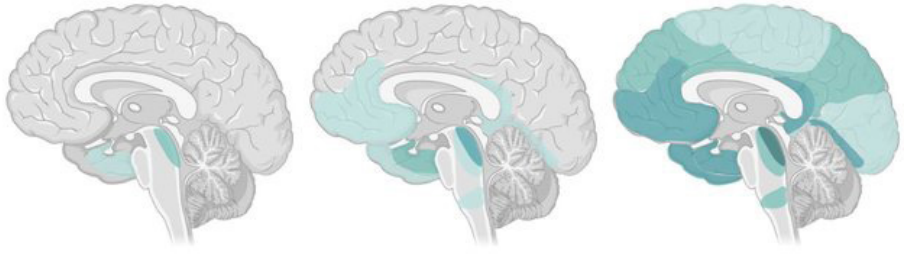

Stages I-II **Stages III-IV** **Stages V-VI**

Figure 2. Braak staging of tau pathology in AD. Representative images showing tau spread from Braak stages I-II (transentorhinal regions) to stages III-IV (limbic regions), and ultimately to stages V-VI (neocortical regions). Figure adapted from Goedert et al. (2016)[19].

Other studies have shown that pathological tau spreading in AD may follow a distinct pattern that does not fit the Braak staging model, depending on the underlying phenotype. For instance, Lowe et al. (2018)[20] examined more brain regions than the ones involved in Braak staging using ^{18}F-flortaucipir and reported variability in regional tangle deposition patterns in early onset AD dementia versus late onset AD dementia. In Vogel et al. (2021)[21], four distinct spatiotemporal trajectories of pathological tau spreading in AD, with different prevalence degrees, were identified using a data-driven subtyping model. While the tau Braak staging system may not fully capture the tau spreading subtypes and may not account for differences in tau spreading at the individual level, it does sufficiently capture tau spreading at the group level in typical AD.

Amyloid-ß PET quantification in *syngo*.MI Neuro Cortical Analysis

Visual assessment by a trained physician is crucial for accurate and reliable reading of amyloid PET images. It allows physicians to differentiate between high and normal cortical amyloid levels and to identify white matter uptake. Visual assessment is the primary form of amyloid PET imaging evaluation. However, accurate characterization of the degree of amyloid deposition in early cases may be difficult with visual estimation only. Loss of grey-white matter differentiation, an early feature in amyloid positive patients, may not always be visually apparent. The combination of visual and quantitative evaluation using SUVr may provide useful information to the reporting physician. Examples of negative and positive Aβ PET scans corresponding to the three available radiotracers are shown in Figure 3.

For over a decade, *syngo*.MI Neuro has had an analysis workflow dedicated to automated SUVr-based quantification of amyloid PET imaging. This workflow, referred to as Cortical Analysis, provides the reading physician with a user-friendly software tool that enables qualitative and quantitative assessments of amyloid PET brain studies with all three approved radiotracers. SUVr computation uses tracer-specific target and reference regions of interest (ROI). The processing pipeline is a PET-only pipeline that was first

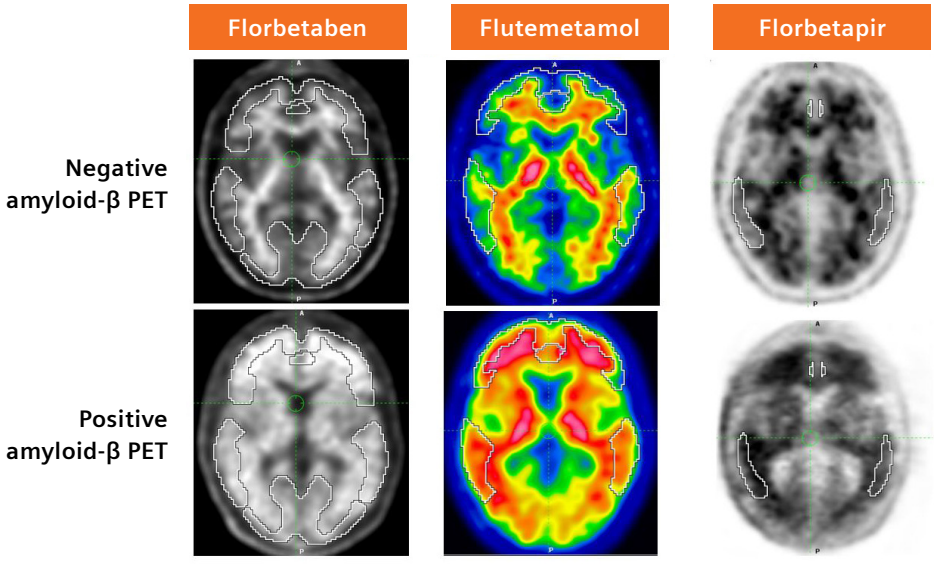

Figure 3. Example of negative (top row) and positive (bottom row) Aβ PET scans corresponding to healthy young subjects and to elderly subjects with AD, respectively. From left to right: florbetaben, flutemetamol, and florbetapir. Tracer-specific cortical regions (white outline) overlaid on each slice. Images displayed using colormaps per the label recommendations. Images publicly available at GAAIN database.

developed to quantify florbetapir scans. It was first introduced and evaluated in Peyrat et al. (2022)[22] where calculated SUVr values were compared with the ones obtained using the method employed in Fleisher et al. (2011)[23] Later, the newly developed quantification method was extended to quantify florbetaben and flutemetamol PET images. The processing steps included a PET-to-PET affine registration of the input PET image to a PET template in the Montreal Neurological Institute (MNI) standard space followed by SUVr calculation using predefined tracer-specific target and reference regions.

These regions, which are tracer-specific, were initially defined from the Automated Anatomical Labeling (AAL) atlas[24] and adapted, following the tracer vendor's recommendations, to match as closely as possible the regions previously used in the tracers' trial studies.[23,25]

For each tracer, a composite SUVr is calculated as the average of individual regional SUVrs corresponding to six predefined cortical regions with respect to a reference region. Table 1 lists the supported cortical target and reference region combinations for each of the three radiotracers, and Figure 4 shows example displays of these regions. As an alternative to the three listed reference regions in Table 1, the user can select from other regions, including the primary visual cortex and the brain stem. It is possible to customize the individual segment boundaries based on the user's preferences to further refine individual segment delineation, which will consequently result in SUVr changes. Note that no changes to the reference region are allowed when calculating CL, as will be discussed later.

Key images and results can be copied or exported and used in a report. In addition, quality control tools for the individual analysis steps, such as the fusion to MNI template, are available during the analysis. For instance, if the default PET-based spatial normalization of the input PET image is inaccurate, manual adjustments can be applied, and, if a CT scan is available, it can be used to guide the spatial normalization of the input PET image to the MNI space using a CT-based affine registration.

Table 1. Tracer-specific cortical and reference regions supported in *syngo*.MI Neuro Cortical Analysis workflow for SUVr calculation.

	Florbetapir	**Florbetaben**	**Flutemetamol**
Target regions	Anterior cingulate gyrus (florbetapir) Frontal lobe (florbetapir) Parietal lobe (florbetapir) Posterior cingulate (florbetapir) Precuneus (florbetapir) Temporal lobe (florbetapir)	Anterior cingulate gyrus (florbetaben) Frontal lobe (florbetaben) Occipital lobe (florbetaben) Parietal lobe (florbetaben) Posterior cingulate (florbetaben) Temporal lobe (florbetaben)	Anterior cingulate gyrus (flutemetamol) Frontal lobe (flutemetamol) Parietal lobe (flutemetamol) Posterior cingulate (flutemetamol) Precuneus (flutemetamol) Temporal lobe (flutemetamol)
Reference region	Cerebellum (florbetapir)	Cerebellar cortex (florbetaben)	Pons (flutemetamol)

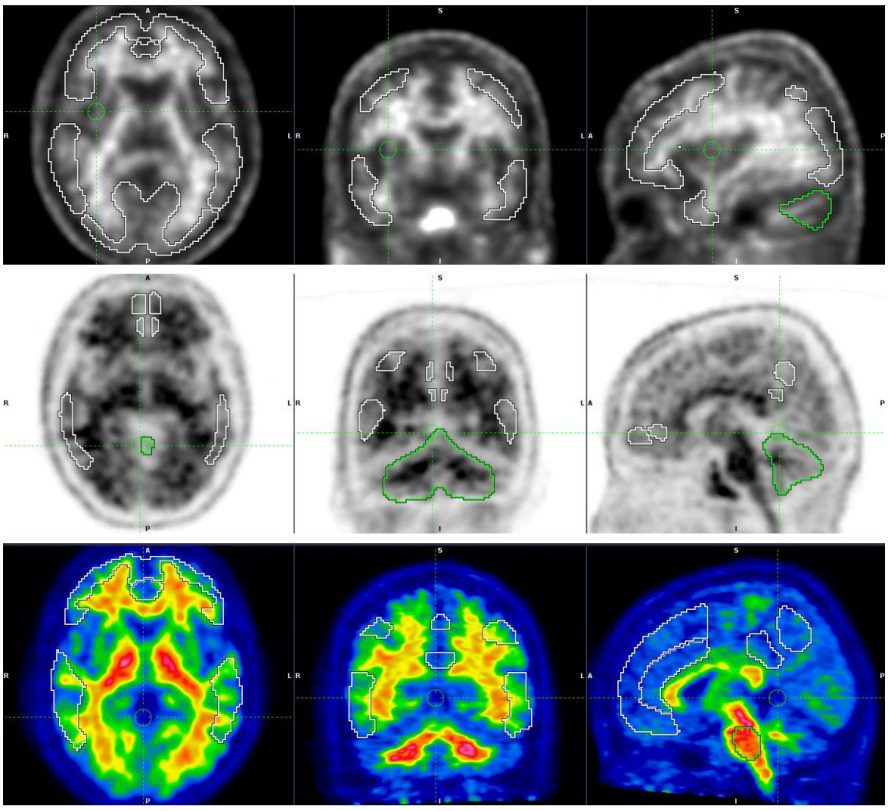

Figure 4. Tracer-specific cortical (white) and background (green) regions in MNI space overlaid on sample PET scans aqcuired by the coresponding radiotracer. From top to bottom: regions correspond to florbetaben, florbetapir, and flutemetamol. The regions sampled by these masks are listed in Table 1. Images courtesy of GAAIN.

Several validation studies[22,26-28] aiming to assess the performance of the implemented Aβ quantification method against established MR-based analysis methods[25, 29-30], some of which were shown to correlate well with autopsy data, have been conducted for the three clinically approved amyloid radiotracers. For example, in Hutton et al. (2015)[26], cortex-to-cerebellum florbetapir SUVr values were calculated with *syngo*.MI Neuro using a diverse clinical population of 604 subjects from the Alzheimer's Disease Neuroimaging Initiative (ADNI)[31] and a group of 74 young, healthy controls. These were compared to SUVrs calculated using an MRI-based method developed by the tracer vendor.[29] The results showed strong correlation and good agreement between the two approaches. In Hutton et al. (2014)[27], *syngo*.MI Neuro cortex-to-cerebellar-gray florbetaben SUVr values were compared against SUVrs calculated with the MRI-based method used in Barthel et al. (2011)[25] with data from the florbetaben phase II trial study (N = 135). There was strong correlation between the two sets of SUVr values. Finally, in Hutton et al. (2014)[28], cortex-to-pons SUVrs calculated with *syngo*.MI Neuro were compared to those calculated using the MRI-based method in Lundqvist et al. (2013)[30] on N = 50 datasets from phase II clinical trial of ^{18}F-flutemetamol. Again, the results showed good correlation between the two approaches.

Amyloid PET-based deformable registration

To account for the wide variability of brain morphology, it is often not possible to accurately align all cortical regions to the standard space using an affine transformation model. To address this issue, a PET-to-PET deformable registration algorithm was later introduced in *syngo*.MI Neuro Cortical Analysis to improve the existing spatial normalization of Aβ PET images to the MNI atlas space.[33] This algorithm is based on a deformable database feature matching (DFM) algorithm that matches points-of-interest (POIs) defined in the patient's native brain against a "template" of POIs in the MNI space. The latter was created as described below:

- Starting from a set of 40 paired amyloid PET and MRI images belonging to subjects with different disease states, each MRI image was first aligned with the MNI space using a deformable registration algorithm using the Statistical Parametric Mapping (SPM) software package.[34] Second, a PET-to-MRI rigid registration was applied to co-register each PET with its paired MRI. The two resulting transformations were then combined to register PET images to the MNI space.

- A set of POIs and their descriptors were then created from the registered PET images. Each POI was detected using an image-based point detection algorithm, and a corresponding feature descriptor was computed to encode the position, scaling, and specific visual characteristics in a neighborhood of the POI.

To register a PET image with the MNI space using the generated POI template, a set of POIs and their descriptors were generated in the patient's space as described above. Then, each POI on the patient image was matched to its closest point in the POI template considering only the POI descriptors. Finally, a geometrical transformation that maximizes the number of truly matched POIs is computed through a distance minimization process. The result is a dense displacement field.

To validate this novel deformable registration algorithm, the Dice coefficient, a measure of overlap, was calculated between brain regions automatically positioned in MNI space using MRI, and the ones transformed from patients' native spaces to MNI space using either the PET-based affine registration or the deformable registration algorithm. The six cortical regions used for florbetapir SUVr calculation were used in this experiment in a group of 39 patients with paired PET and MRI scans. The deformable registration resulted in a larger number of cases with higher overlap compared with the affine registration as shown in Figure 5. The graph shows that, in more than half of the cases (27/39), regions of interest overlapped by 70% of the region volume following deformable registration, but only 7/39 cases when using affine registration. This result demonstrates that the induced PET-based deformable registration can match brain anatomical regions with their counterparts in the template brain more accurately, even for small size regions.

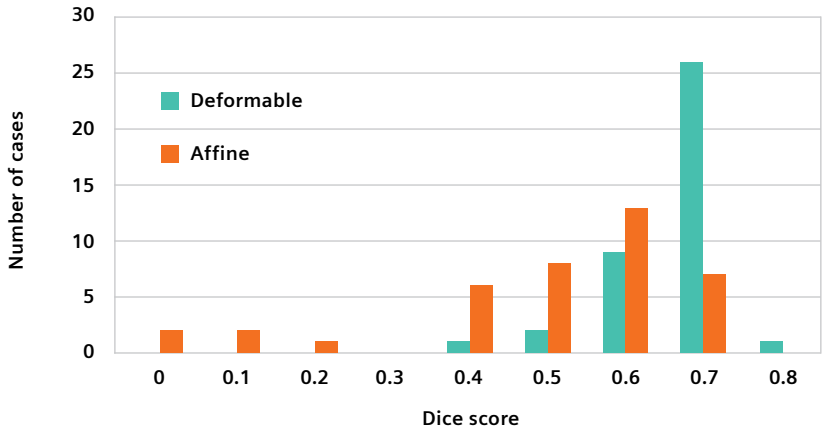

Figure 5. Dice score representing percent volume of overlap between regions of interest positioned automatically in template space using MRI and those resulting from deformable and affine registration of PET images for 39 florbetapir PET scans.

In addition, a comparison of cortex-to-cerebellum SUVrs calculated with *syngo*.MI Neuro using the deformable registration algorithm against those calculated in Fleisher et al. (2011),[23] which also uses a non-linear registration to an MNI template, was conducted using N = 604 florbetapir cases from ADNI. Correlation between the two sets of SUVr values was very strong with $R^2 = 0.99$ and the following linear regression of DFM SUVr values on those reported in Fleisher et al. (2011)[23]: $y = 1.03 \times x - 0.01$, which can be used to convert the SUVr threshold for florbetapir PET positivity (SUVr > 1.10[23,29]) to a corresponding threshold for *syngo*.MI Neuro of 1.12.

Standardization using the Centiloid scale

The CL method was proposed in Klunk et al. (2015)[2] to standardize Aβ PET measures, such as the SUVr, across various amyloid PET tracers and analysis methods and to provide a standardized scale that can be used to improve comparability of amyloid PET quantification and define common normative ranges. The CL method allows amyloid PET measures to be transformed into standard CL units using a two-step calibration process. SUVr values, corresponding to a given ^{18}F-labeled tracer and calculated using a given processing pipeline, are calibrated to match those of ^{11}C-PiB, which are then transformed into the CL scale.

CL calibration was recently added to *syngo*.MI Neuro Cortical Analysis workflow for the three commercially available amyloid radiotracers to allow direct conversion of composite SUVr values to the CL scale using tracer-specific target regions (Table 1) with reference to the whole cerebellum, as described in the following sections.

Centiloid equations

To generate tracer-specific SUVr-to-CL conversion equations, PET images corresponding to young control 0-anchor (YC-0) and AD 100-anchor (AD-100) patients for the selected tracer, and their corresponding paired ^{11}C-PiB images were obtained from the open-source Global Alzheimer's Association Interactive Network (GAAIN) CL project website.[35] For each tracer, GAAIN data consist of a pair of PiB- and ^{18}F-based tracer datasets corresponding to 46 ^{18}F-florbetapir (13 YC and 33 AD), 35 ^{18}F-florbetaben (10 YC and 25 AD), and 74 ^{18}F-flutemetamol scans (24 YC and 50 AD).

Level 2 calibration analysis[2] was performed to generate direct SUVr-to-CL transformations using the three tracer-specific cortical regions and the same cerebellar region in *syngo*.MI Neuro Cortical Analysis (Table 2).

For each tracer, the obtained YC-0 and AD-100 images were processed using the *syngo*.MI Neuro Cortical Analysis workflow and the generated SUVr values (^{Tracer}SUVr) were regressed against their corresponding published[35] ^{PiB}SUVr values (^{PiB}SUVr). The acceptance criterion for this regression is $R^2 > 0.7$.[2] The resulting regression equation, with slope $^{Tracer}a$ and intercept $^{Tracer}b$,

$$^{Tracer}SUVr = {}^{Tracer}a \times {}^{PiB}SUVr + {}^{Tracer}b \qquad \text{(Equation 1)}$$

is then used to convert ^{Tracer}SUVr into calculated PiB SUVrs, $^{Calc\text{-}PiB}$SUVr, as follows:

$$^{Calc\text{-}PiB}SUVr = \frac{{}^{Tracer}SUVr - {}^{Tracer}b}{{}^{Tracer}a} \qquad \text{(Equation 2)}$$

which can then be inserted in the CL equation[1]:

$$^{Tracer}CL = \frac{^{Calc\text{-}PiB}SUVr - {}^{YC-0}_{PiB}SUVr}{{}^{AD-100}_{PiB}SUVr - {}^{YC-0}_{PiB}SUVr} \times 100 \qquad \text{(Equation 3)}$$

where the reference values $^{YC-0}_{PiB}SUVr$ and $^{AD-100}_{PiB}SUVr$ correspond to the mean PiB SUVr values for the 0-anchor (YC-0) (N = 34) and the AD 100-anchor (AD-100) (N = 45) subject sets, respectively. These mean values are determined using the 50-70 min PiB data and the standard cortical region published by GAAIN for different reference regions.[2,34] For example, when a cerebellar reference region is used, then

$$^{Tracer}CL = \frac{^{Calc\text{-}PiB}SUVr - 1.009}{1.067} \times 100$$

This allows the conversion of $^{Tracer}SUVr$ to $^{Tracer}CL$ for each YC-0 and AD-100 subject by substituting $^{Calc\text{-}PiB}SUVr$ (Equation 2) and the appropriate mean values $^{YC-0}_{PiB}SUVr$ and $^{AD-100}_{PiB}SUVr$ in Equation 3. The final SUVr-to-CL conversion equation is then generated by regressing the SUVr values against the CL values for all YC-0 and AD-100 subjects. This process was repeated for each tracer using its corresponding cortical regions and the whole cerebellum as the reference region to generate the conversion equations shown in Table 2.

Table 2. *syngo*.MI Neuro Cortical Analysis Centiloid calibration equations using tracer-specific target regions (see Table 1) with reference to the same whole cerebellar region.

Tracer	$^{Calc\text{-}PiB}SUVr^{*}$	$R^{2\,(a)}$	SUVr-to-CL equation	$R^{2\,(b)}$
Florbetapir	(^{Tracer}SUVr – 0.458)/0.547	0.878	171.49 × ^{Tracer}SUVr – 173.04	0.969
Florbetaben	(^{Tracer}SUVr – 0.448)/0.517	0.939	181.42 × ^{Tracer}SUVr – 175.84	0.981
Flutemetamol	(^{Tracer}SUVr – 0.187)/0.773	0.946	121.20 × ^{Tracer}SUVr – 117.24	0.968

* Calculated PiB SUVr value as given by Equation 2.
a: corresponding to the regression of PiB calculated SUVrs (Equation 2) against published PiB SUVrs.[35] All values are > 0.7.
b: corresponding to the regression of *syngo*.MI Neuro Centiloid values against published GAAIN counterparts.[2,35]

Figure 6 illustrates how users can select the appropriate target and reference regions for each radiotracer. If a configuration other than the three supported configurations in Table 2 is selected, only SUVr values are calculated and reported, not the CL value. Figures 7-8 show examples of amyloid scans with high and low amyloid uptake with corresponding CL values.

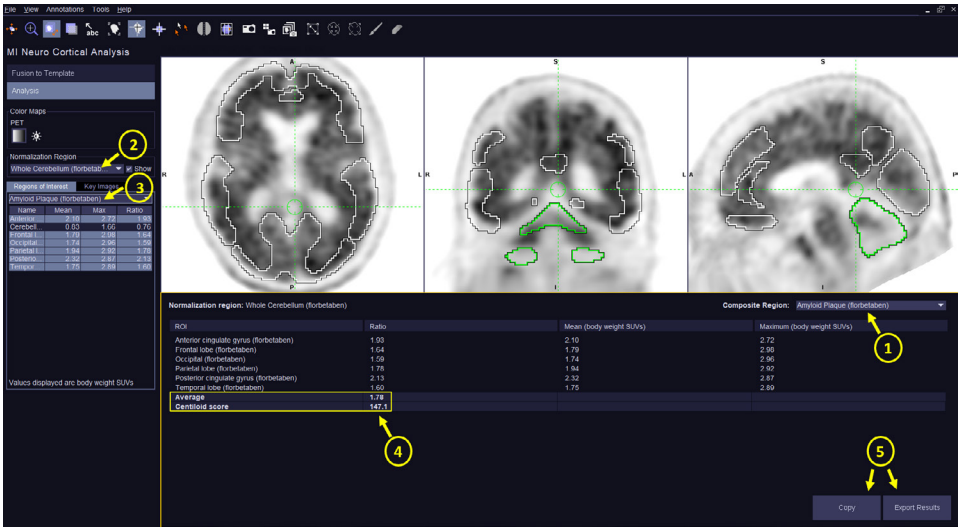

Figure 6. *syngo*.MI Neuro Cortical Analysis user interface for amyloid PET quantification. Dropdown menus shown by arrows 1 and 2 can be used to select one of the appropriate combinations of "target/reference" regions for SUVr and CL calculations. Unlike SUVr values, CLs are only calculated when the tracer-specific target regions (Table 1) with a cerebellar reference region are selected. Dropdown menu 3 can be used to match the Composite Region selection in 1. Each of these regions can be shown overlaid on the PET image when clicked on (white contours: target regions; green: reference region). Calculated composite SUVr and corresponding CL values are shown by arrow 4, which can be copied or exported as a csv file using buttons shown by arrows 5. Images courtesy of GAAIN.

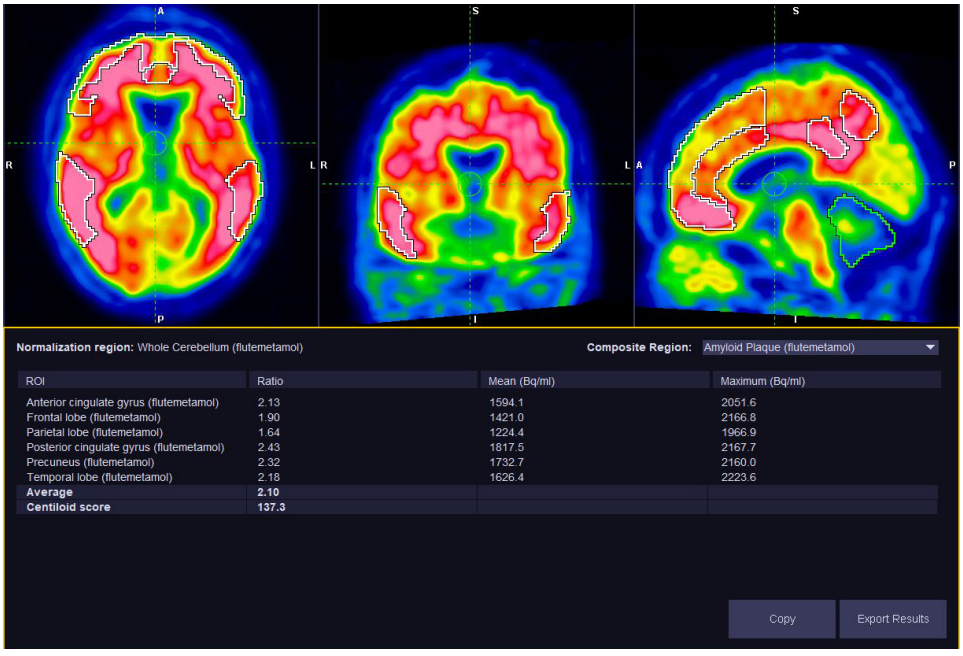

Figure 7. Example of a positive flutemetamol scan of a patient with AD processed with *syngo*.MI Neuro Cortical Analysis. High cortical uptake with a composite cortex-to-whole cerebellum SUVr of 2.10 and a corresponding CL value of 137.3. Images courtesy of GAAIN.

Figure 8. Example of a negative florbetaben scan of a young healthy subject, processed with *syngo*.MI Neurology Cortical Analysis with a composite cortex-to-whole cerebellum SUVr of 0.97 and a corresponding CL value of 0.1. Images courtesy of GAAIN.

Validation using GAAIN datasets

The generated SUVr-to-CL calibration equations were used to compare *syngo*.MI Neuro CL values against their published GAAIN counterparts. Corresponding regression and Bland-Altman plots are shown on Figure 9 for each tracer using tracer-specific cortical regions and the whole cerebellum as the background region. These plots show strong correlations and good agreements between the compared sets of CL values across all tracers.

Validation with independent datasets

Two additional experiments were performed to validate the derived CL equations. In the first validation experiment[36], CL values were calculated with *syngo*.MI Neuro Cortical Analysis using a set of amyloid scans obtained from the ADNI database and were compared to publicly available CL values calculated using ADNI processing pipeline with a whole cerebellum reference region. The selected ADNI scans correspond to multi-time point exams from N = 289 subjects including elderly healthy controls, MCI patients, and AD patients, for a total of 162 ^{18}F-florbetapir and 150 ^{18}F-florbetaben scans.

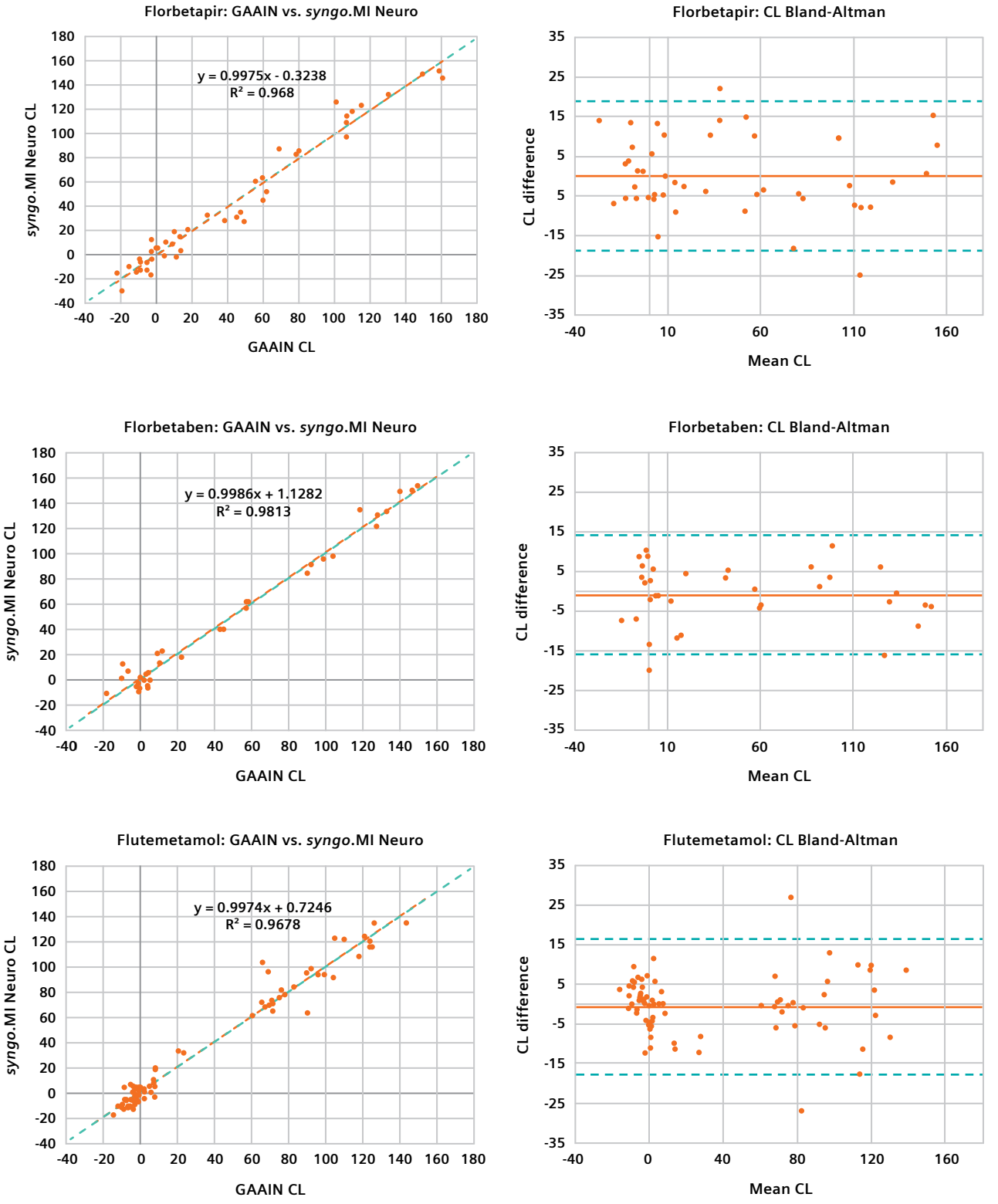

Figure 9. Performance evaluation of *syngo*.MI Neuro Cortical Analysis. Comparison of *syngo*.MI Neuro values with published GAAIN counterparts for each tracer. *syngo*.MI Neuro values correspond to tracer-specific cortical regions and whole cerebellum as reference region. Upper and lower limits (UL and LL) of Bland-Altman plots correspond to "bias ± 1.96 × SD of CL difference": (florbetapir: UL = 15.03 CL and -LL = 18.24 CL with bias = -0.044; florbetaben: UL = 20.34 CL and LL = -12.24 CL with bias = -1.005; and flutemetamol: UL = 16.56 CL and LL = -17.83 CL with bias = -0.60). SD: standard deviation.

Comparisons between the two sets of CL values are show in in Figure 10 with high correlations ($R^2 > 0.97$) and good agreements for both tracers.

The second validation experiment[37] was performed in collaboration with Clínica Universidad de Navarra in Spain using a multi-site cohort of patients (N = 162; 69 females and 93 males; age: 71.3 ± 6.2 years). Each patient underwent an amyloid PET exam using one of the three commercially available amyloid PET radiotracers with a total of 21 ^{18}F-florbetaben, 51 ^{18}F-flutemetamol, and 90 ^{18}F-florbetapir scans. All scans were acquired on a Biograph mCT scanner following standard tracer-specific protocols. Images were reconstructed using the ordered subset expectation maximization (OSEM) method with time-of-flight (TOF) and point-spread-function (PSF) corrections, 3 iterations, 21 subsets, 2 mm post-reconstruction Gaussian smoothing, zoom factor of 2, and a 400 × 400 matrix. Reconstructed images were visually rated as amyloid "positive" or "negative" through consensus by two trained nuclear medicine physicians using tracer-specific visual reading guidelines. CL values were calculated with *syngo*.MI Neuro Cortical Analysis using tracer-specific equations in Table 2.

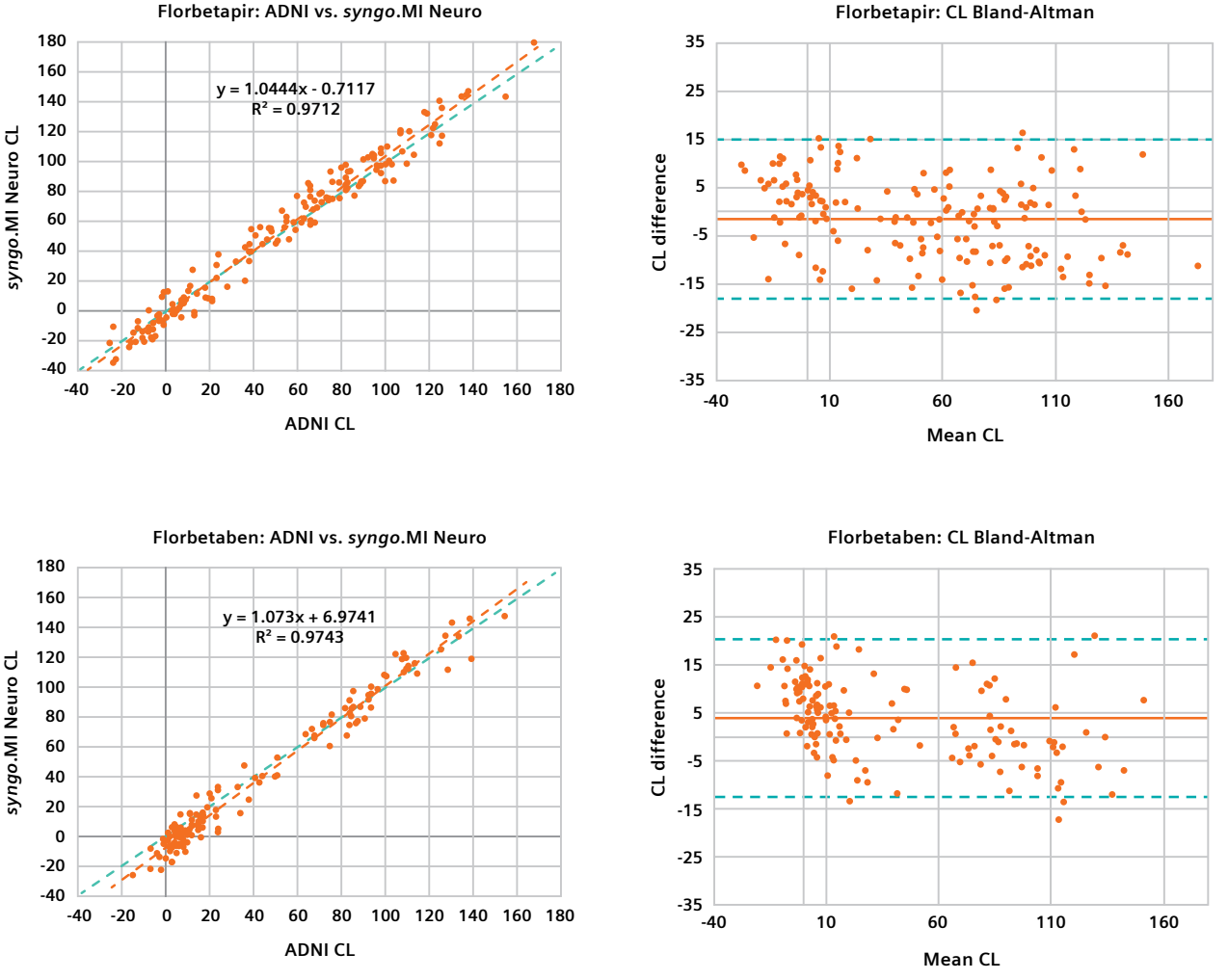

Figure 10. Comparison of CL values calculated with *syngo*.MI Neuro Cortical Analysis against their publicly available ADNI counterparts. The upper and lower limits (UL and LL) of Bland-Altman plots correspond to 'bias ± 1.96 × SD of CL difference' (florbetapir: UL = 15.03 CL and LL = -18.24 CL with bias = -1.60; florbetaben: UL = 20.34 CL and LL = -12.24 CL with bias = 4.05). SD: standard deviation.

A receiver operating characteristic (ROC) analysis was performed to discriminate patients in agreement with the visual reading used as gold standard. A CL cut-off value was determined as the value that maximized the Youden's J Index of the ROC curve.

The percentage of concordance between readers was 95% with eight discordant cases that were excluded from the ROC analysis. Most cases (N = 107 or 66%) were visually classified as positive and had a mean CL of 67.8 ± 29.2 CL, while subjects visually classified as negative exhibited significantly lower CL values with a mean of -3.0 ± 20.9 CL ($p < 0.05$). An area under the ROC curve of 0.9786 was obtained with a corresponding CL cut-off value of 28 CL (sensitivity 91.6% and specificity 94.6%), indicating high agreement with visual read-based classification as shown on Figure 11-left. Figure 11-right, on the other hand, shows the breakdown of concordant and discordant cases between visual and CL-based classification into positive and negative amyloid scans using 28 CL as the cut-off point.

CL values corresponding to most discordant cases (i.e., V+Q- or V-Q+) fall in an intermediate CL range of approximately 10 to 50 CL that includes both visually positive and negative cases, indicating that such cases are more challenging to interpret both visually and quantitatively.

Finally, to assess if the choice of reference region has an impact on CL values and cut-offs, the same classification experiment as above was performed using the pons and a cerebellar gray region region for flutemetamol and florbetaben scans, respectively, instead of the whole cerebellum which was used only for florbetapir scans. In this case, a cutoff point of 26 CL was obtained with AUC = 0.987, sensitivity = 92.0%, and specificity = 96.3%. Note that both determined CL thresholds are comparable to those published previously.[38-39]

The choice of reference region has been reported to have a great impact on CL values, with the pons resulting in the lowest mean CL values across the entire amyloid burden range.[42] In addition, due to their relatively small sizes and each consisting of one tissue type, the PET signal within the pons and the cerebellar cortex is more affected by motion and partial volume effect, making them more sensitive to scan harmonization

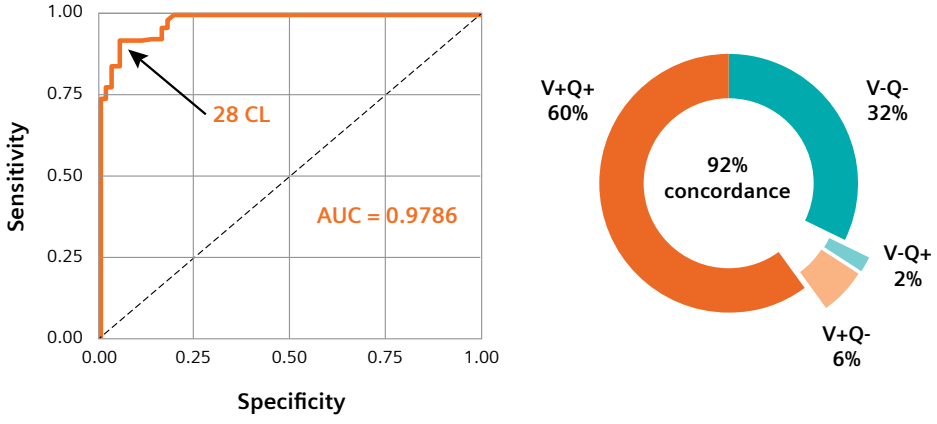

Figure 11. Left: receiver operating characteristic (ROC) curve showing strong agreement between CL- and visual read-based classifications with an area under the curve of 0.9786 with a sensitivity of 91.6% and a specificity of 94.6%. Right: breakdown of concordant and discordant cases between visually and quantitatively classified subjects as amyloid positive or negative (using a cutoff point of 28 CL). A 92.2% concordance was achieved. V: visual read and Q: quantification.

compared to the whole cerebellum.[42] For these reasons, it is recommended to use the whole cerebellum reference region for CL calculation in multi-center and in longitudinal studies, especially if PET scans are not properly harmonized.[42] It is also highly recommended to keep the entire CL calculation pipeline consistent (including radiotracer and imaging protocol) whenever possible to avoid biases when comparing patient scans over time.

For more information on CL robustness to image reconstruction, image resolution, reference regions, and more, one can refer for example to the following publications[39-42].

Quantification of ^{18}F-flortaucipir PET in *syngo*.MI Neuro Cortical Analysis

^{18}F-flortaucipir was granted FDA approval in mid-2020 to estimate the density and distribution of aggregated tau NFTs in adult patients with cognitive impairment who are being evaluated for AD. ^{18}F-flortaucipir can accurately detect AD-type tau pathology in more advanced Braak stages with 87.5% accuracy.[43] Per the vendor's recommendations, ^{18}F-flortaucipir image acquisition starts approximately 80 minutes post intravenous injection of the tracer and lasts for 20 minutes. Images are often acquired as four 5-minute dynamic frames with the patient's head positioned such that the entire brain, with the cerebellum, is in the PET scanner field of view.

According to the radiotracer label[44], the clinical interpretation of a ^{18}F-flortaucipir PET scans is primarily based on visual assessment designed to locate neocortical brain regions with tracer activity greater than a measured visual positivity threshold using the average uptake within a manually drawn cerebellar region. Using this method, scans are visually classified as either tau positive (T+) or tau negative (T-) depending on neocortical activity in either hemisphere in posterolateral temporal, occipital, or parietal/precuneus region(s), with or without frontal activity.[44]

Quantification of ^{18}F-flortaucipir PET images using SUVr is often performed in research studies and in clinical trials to measure tau burden in cortical regions with respect to a reference region void of tau accumulation. For example, in the phase 3 trial of the anti-amyloid drug, donanemab[45], tau SUVr was used to confirm AD pathology and to stratify participants into low and high tau cohorts. Participants with an SUVr greater than 1.10 or with a visual positive read were excluded from the trial.

Prior to calculating SUVr values, the acquired PET frames are often motion- and time-corrected to address patient motion and differences in the delay from injection to scan acquisition time across different scans, respectively. The corrected frames are then summed to generate a static image, which is used for regional SUVr calculation. This calculation is performed using either segmented brain regions from a structural MRI scan[46] after co-registering it with the PET scan, or on predefined regions of interest on a standard atlas after warping the PET image onto the atlas space.

A (MRI-free) PET-only quantification solution dedicated to ^{18}F-flortaucipir PET images was recently added to *syngo*.MI Neuro Cortical Analysis workflow. The method calculates volume-weighted SUVr values within predefined individual and composite cortical regions with respect to an inferior cerebellar gray region. This process, depicted in Figure 12, is based on spatial normalization of the input PET image to the MNI space followed by the automatic placement of predefined cortical and reference regions for SUVr calculation as explained in the following sections.

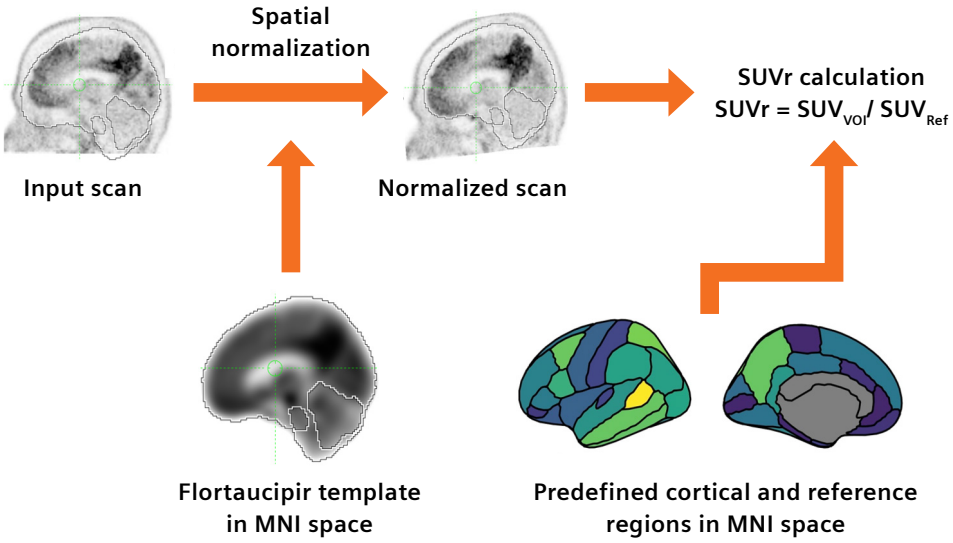

Figure 12: ^{18}F-flortaucipir quantification pipeline using *syngo*.MI Neuro Cortical Analysis. The input PET image is spatially normalized to the MNI space using a deformable registration, then SUVr values are calculated on predefined cortical regions with respect to an inferior cerebellar gray region.

Spatial normalization

Spatial normalization of ^{18}F-flortaucipir PET images in *syngo*.MI Neuro Cortical Analysis is done in two steps using an affine transformation followed by a deformable alignment. The latter is an extension of the DFM algorithm previously developed to register amyloid PET images to MNI space as described above.[33] This algorithm calculates a dense displacement field by matching POIs in the patient's native space against a template of POIs in the MNI standard space. The POI database for ^{18}F-flortaucipir was created using a set of tau (^{18}F-flortaucipir) and amyloid (^{18}F-florbetapir) paired PET images from 40 subjects representing three diagnostic groups: healthy controls, MCI, and AD. The data was all obtained from the ADNI database and was processed as follows.

For each subject, the amyloid image was first registered to MNI space using the existing amyloid-based DFM algorithm, and the resulting transformation guided the registration of the corresponding ^{18}F-flortaucipir image to MNI geometry. Using a point detector method, an atlas of POIs was generated, and their local feature descriptors calculated on the forty spatially normalized tau images in MNI space. For visual assessment, a ^{18}F-flortaucipir reference brain in the MNI space was also created as an average of the forty registered ^{18}F-flortaucipir images.

Target regions and volume-weighted SUVrs

Within the *syngo*.MI Neuro Cortical Analysis workflow, an input ^{18}F-flortaucipir image is first spatially normalized to MNI geometry, as described above, followed by automatic application of a set of predefined brain region masks in MNI space onto the spatially normalized image. These regions represent the six Braak stages, a temporal meta-ROI, and an early-tau region. SUVr values weighted by the size of each region are then calculated with respect to an inferior cerebellar cortex region. The inferior cerebellum was chosen as reference region to avoid tracer bleeding-in from nearby cortical regions to the superior portion of the cerebellum.[47] The implemented cortical and reference regions were all defined based on existing regions in the AAL atlas. The Braak regions (I-VI) are defined based on the definitions adopted in Baker et al. (2017)[47]

The temporal meta-ROI was first introduced to quantify tau PET in Jack et al.[49] It combines regions from the MTL, site of early and high tau deposition in AD, with neocortical regions, which makes it well-suited to capture the distinction between primary age-related tau (PART) and AD. The temporal meta-ROI was shown to better discriminate between AD and non-AD neurodegenerative diseases.[50] The early-tau region was introduced in an autopsy-confirmed study[51] as being a good choice for detecting cognitively impaired subjects in early stages of AD.

Note that the hippocampus was excluded from the temporal meta-ROI and from the early-tau region because of frequent bleed-in from off-target binding in the choroid plexus. Definitions of all these regions are given in Table 3.

For each (individual or composite) target region, the SUVr value is calculated as a volume-weighted average of SUVrs within the left and right sides of each of its sub-regions, as follows:

$$SUVr_W = \frac{(SUVr_1 \cdot Volume_1 + SUVr_2 \cdot Volume_2 + \cdots + SUVr_n \cdot Volume_n)}{(Volume_1 + Volume_2 + \cdots + Volume_n)}$$

where, $SUVr_n$ refers to the SUVr value in the n^{th} sub-region and $Volume_n$ denotes its volume measured as its total number of voxels. Note that the formula does not explicitly distinguish between the left and right sides of each region, but this is incorporated in the implementation. The software also allows computation and exporting of volume-weighted SUVrs within the following composite regions: Braak I-II, Braak III-IV, Braak V-VI, and Braak I-VI.

Table 3. Cortical regions used in *syngo*.MI Neuro Cortical Analysis for SUVr calculation with ^{18}F-flortaucipir images.

Region	Definition	Braak stage
Braak I	Entorhinal cortex	Transentorhinal
Braak II	Hippocampus	
Braak III	Amygdala, parahippocampal gyrus, fusiform gyrus, and lingual gyrus	Limbic
Braak IV	Caudal anterior cingulate gyrus, inferior temporal gyrus, Insula, isthmus cingulate gyrus, middle temporal gyrus, posterior cingulate gyrus, rostral anterior cingulate gyrus, and temporal pole	
Braak V	Caudal and rostral middle frontal gyri, frontal pole, inferior parietal gyrus, lateral occipital lobe, medial orbitofrontal gyrus, pars opercularis, pars orbitalis, pars triangularis, precuneus, superior frontal gyrus, superior parietal gyrus, superior temporal gyrus, and supramarginal gyrus	Neocortical
Braak VI	Cuneus, paracentral, pericalcarine, postcentral, and precentral cortices	
Early tau	Entorhinal cortex, fusiform gyrus, inferior temporal gyrus, and parahippocampal gyrus	
Temporal meta-ROI	Amygdala, entorhinal cortex, fusiform gyrus, inferior temporal gyrus, middle temporal gyrus, and parahippocampal gyrus	

Examples of ^{18}F-flortaucipir images showing different uptake patterns are shown in Figures 13-15.

Figure 13. A 56-year-old A-/T- (per visual reads), female with MCI. Low uptake throughout with some off target binding in the striatum and part of the meninges. Low SUVr values in all Braak regions with a mean SUVr = 1.10, with a relatively higher Braak II (hippocampus) with SUVr = 1.20, which can be attributed to spill-in from neighboring choroid plexus. Data from the A05 trial.

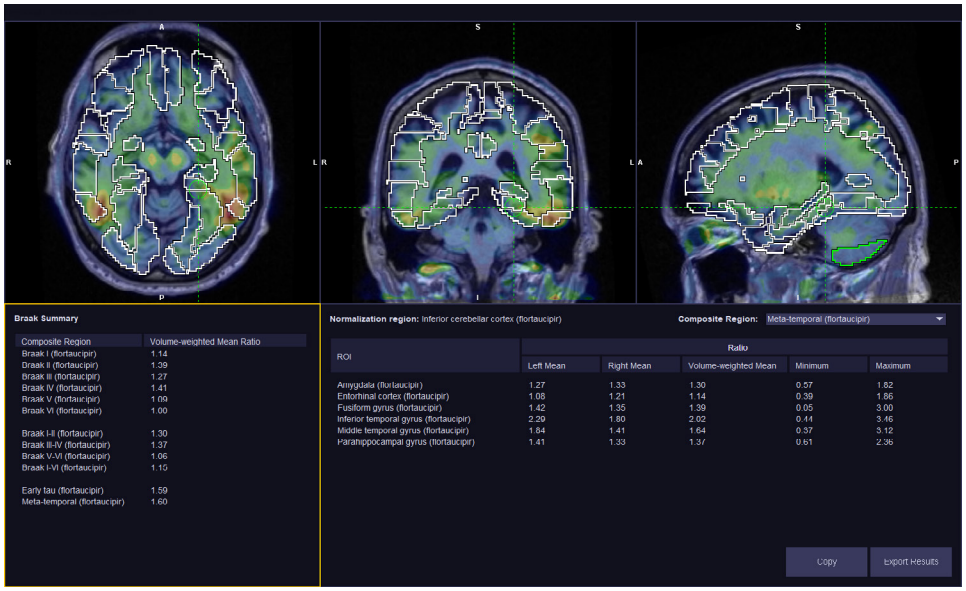

Figure 14. A 74-year-old A+/T+ (per visual reads) male with MCI. Abnormal and asymmetric ^{18}F-flortaucipir uptake in the inferior temporal gyrus, the temporal pole, inferior parietal, and lateral occipital, with SUVr values for Braak I-II, Braak III-IV and Braak V-VI equal to 1.30, 1.37, and 1.06, respectively. Data from the A05 trial.

Figure 15. A 54-year-old A+/T+ (per visual reads) female with AD. Increased ^{18}F-flortaucipir uptake in all major lobes including the frontal and occipital lobes where tau accumulates at later stages of the disease. High SUVr at all Braak regions with Braak I-VI SUVr = 1.83 and the SUVr for the temporal meta region equal to 2.21. Data from the A05 trial.

Comparison with an MRI-based quantification method

Volume-weighted SUVr values calculated using the *syngo*.MI Neuro Cortical Analysis workflow on a set of ^{18}F-flortaucipir PET images (N = 717), obtained from ADNI, were compared to values calculated using an MRI-based quantification pipeline.[48,52] The latter is based on co-registering each tau PET scan to its corresponding MRI image, which is bias-corrected and segmented using *Freesurfer* (https://surfer.nmr.mgh.harvard.edu/) to define ROIs for SUVr calculation. To span a variety of uptake density and patterns, the ADNI ^{18}F-flortaucipir scans represent three diagnostic groups: normal control, MCI, and AD. For each scan, cortex-to-inferior cerebellar grey volume-weighted SUVrs were calculated using *syngo*.MI Neuro Cortical Analysis and were compared to volume-weighted SUVrs calculated using ADNI's MRI-based quantification method (publicly available on ADNI website). Comparisons were performed on individual and composite regions.

The following regression and Bland-Altman plots (Figure 16) show moderate to good correlations between the two sets of SUVr values calculated on different composite regions. Note the lowest R^2 value for Braak I-II (R^2 = 0.86), which is most likely due to the small size of the entorhinal cortex and the hippocampus, as well as the spill-in from the choroid plexus to the hippocampus.

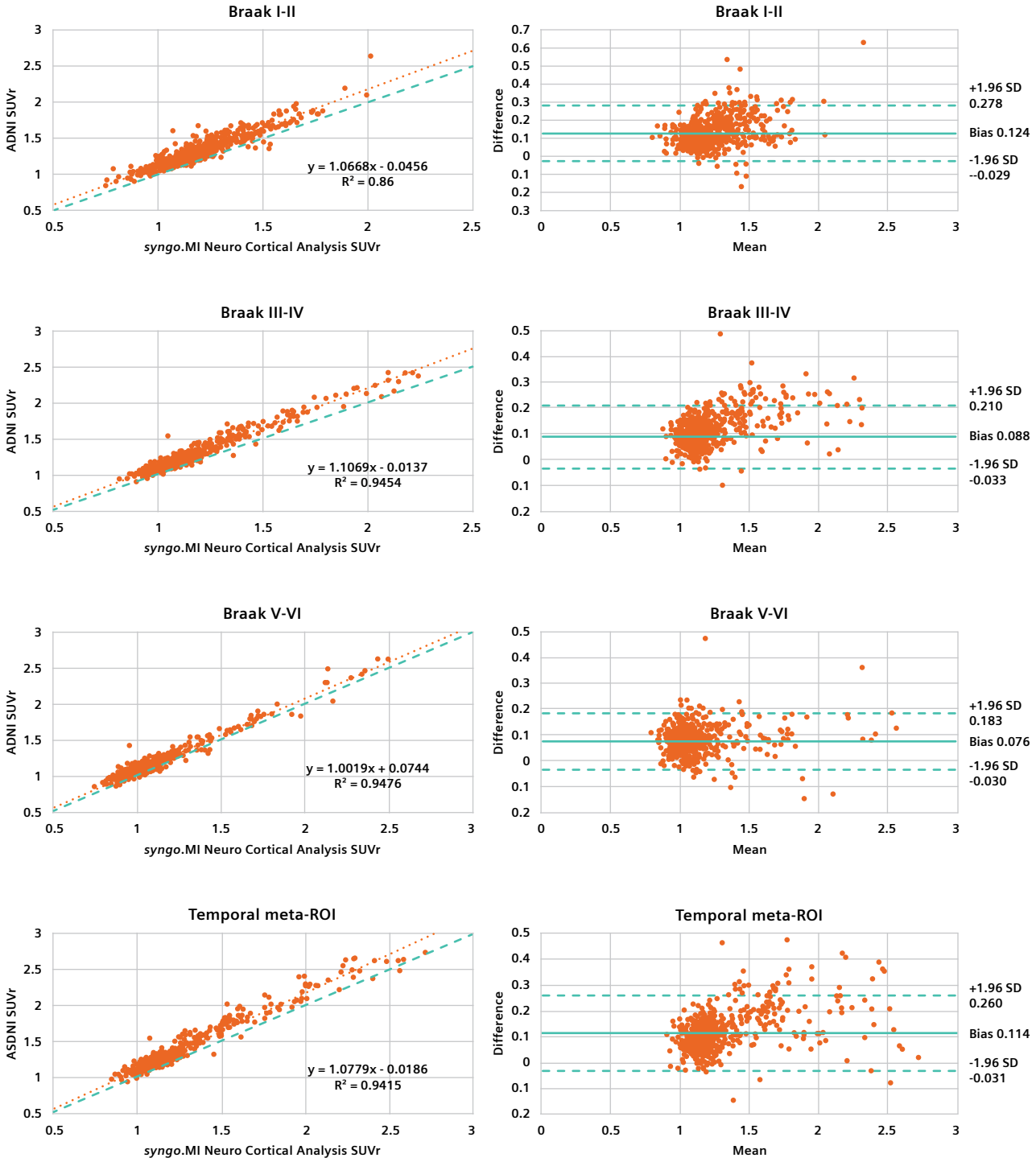

Figure 16. Cortex-to-cerebellar gray volume-weighted SUVrs calculated using *syngo*.MI Neuro Cortical Analysis compared to their counterparts calculated using the MRI-based ADNI method on N = 717 ^{18}F-flortaucipir scans for different brain composite regions. (Left) regression and (right) Bland-Altman plots for each region.

Additional comparisons of volume-weighted regional SUVr values calculated on individual regions are presented in Figure 17 for the precuneus, the inferior temporal gyrus, the lingual gyrus, and the amygdala. These show strong correlations between the two sets of SUVr values.

These cross-validation results demonstrate good alignment, at both the composite and individual ROI level, of the introduced PET-only quantification method with an established MRI-based analysis method.

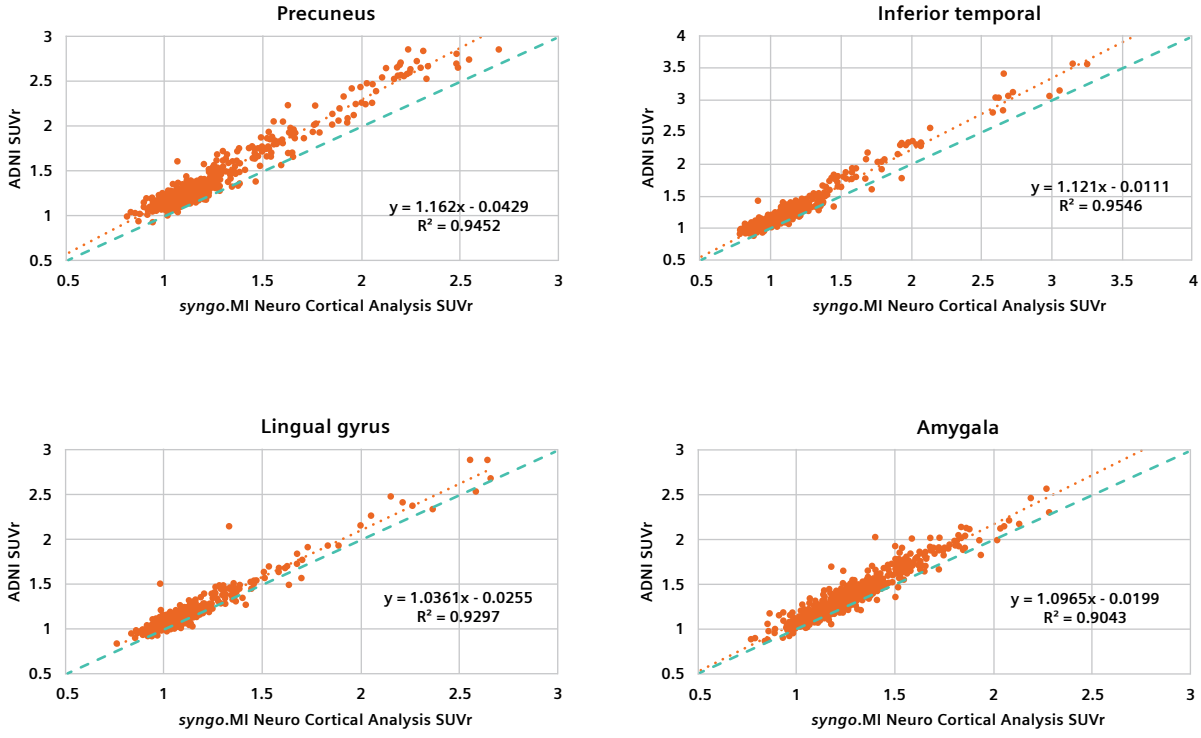

Figure 17. Cortex-to-cerebellar gray volume-weighted SUVrs calculated using *syngo*.MI Neuro Cortical Analysis compared to their counterparts calculated using the MRI-based ADNI method (N = 717) for different individual brain regions.

Tau Positivity (T+) thresholds

Per the radiotracer label, a ^{18}F-flortaucipir PET scan is visually classified as either positive (T+) or negative (T-) according to the approved visual read guidelines, which require a certain level of expertise and can be limiting for large multi-center studies. In research settings and in large AD modifying therapy trials, ^{18}F-flortaucipir PET images are also interpreted using semi-automated quantification tools based on SUVr calculation, and tau positivity is often determined through comparison to a cohort-based SUVr threshold.[53] As a result, various SUVr-based ^{18}F-flortaucipir cut-points have been proposed for tau positivity.[16,20,43,49,53-56] These cut-points differ depending on the processing method, the brain regions used for SUVr calculations, the clinical and

demographic characteristics of the reference cohort, and the analytical approach used to define the cutoff points (e.g., receiver operating characteristics (ROC) with Youden's J index or as two standard deviations above the mean SUVr (*mean+2xSD*) of the reference cohort).

In addition, ROIs often used for SUVr calculation, such as the temporal meta-ROI, don't include any of the parietal/precuneus or occipital structures used in the manufacturer's recommended visual interpretation of ^{18}F-flortaucipir scans. Recent studies have investigated the agreement between visual interpretation and SUVr-based quantification (e.g., Chen et al. [2023][56]).

^{18}F-flortaucipir positivity thresholds in *syngo*.MI Neuro Cortical Analysis

To determine tau positivity thresholds for the composite volumes of interest supported in *syngo*.MI Neuro Cortical Analysis, a cohort of N = 189 ^{18}F-flortaucipir exams from the A05 (NCT02016560) observational study was used (Table 4; 15 young controls (YC), 48 elderly cognitively unimpaired (eCU), 85 MCI, and 41 subjects with AD). Each patient had an amyloid (florbetapir) and a tau (^{18}F-flortaucipir) PET scan. Subjects were visually classified as amyloid and tau positive or negative (A+/A- and T+/T-) using the standard reading guidelines for each tracer.

Tau scans were acquired with a single intravenous bolus injection target dose of 370 MBq (10 mCi) of ^{18}F-flortaucipir followed by a saline flush. A continuous 20-minute brain scan (four 5-minute frames) was collected about 80 minutes post injection. For each scan, the four dynamic frames were co-registered to the first frame and summed to generate a static image. The latter was then processed to calculate volume-weighted SUVr values within Braak I-II, Braak III-IV, Braak V-VI, the temporal meta-ROI, and the early tau composite regions, with respect to the inferior cerebellar gray region, as described above. SUVr value distribution for these regions and across diagnostic groups are shown in Figure 18.

Table 4. A05 cohort demographics. Some values are given as mean (std).

	YC	eCU	MCI	AD
N	15	48	85	41
Age (years)	28.3 (4.2)	67.8 (9.9)	70.4 (9.6)	75.5 (8.4)
Sex (M/F)	9/6	24/24	44/41	18/23
MMSE	29.6 (0.51)	29.56 (0.5)	27.72 (1.76)	21.46 (3.93)
ADAS Cog-11	4.2 (2.6)	5.6 (2.9)	10.5 (4.5)	20.1 (8.6)
Visual A+ (%)	0	10.4	48.2	65*
Visual T+ (%)	0	4.1	34.1	51.2

*One case did not have a florbetapir scan.

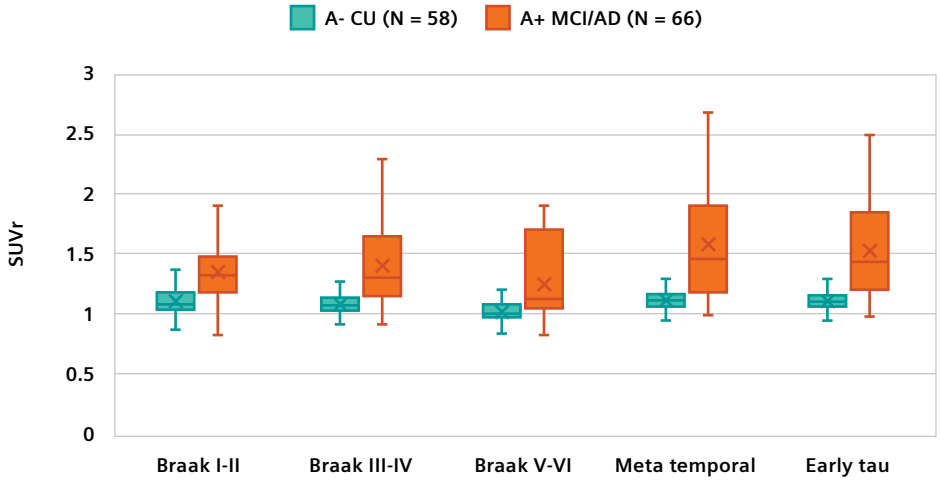

Figure 18. SUVr value distribution for amyloid negative (A-) cognitively unimpaired (young and elderly combined) and amyloid positive (A+) cognitively impaired (MCI and AD) subjects calculated on the five considered composite regions.

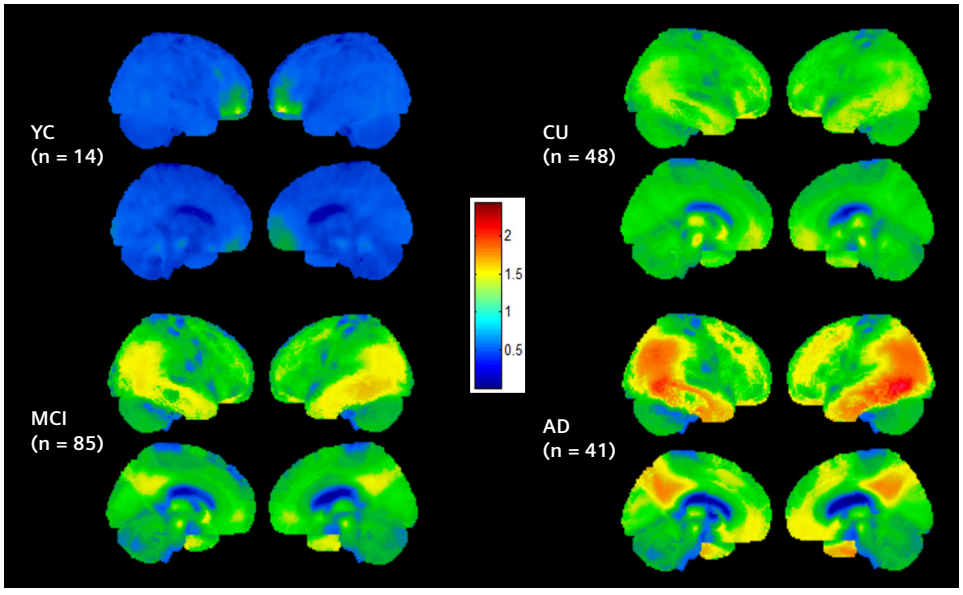

Figure 19. Average SUVr images across the considered diagnostic groups. Right and left lateral and medial views are shown. SUVr values were calculated using an inferior cerebellar cortex region as reference. YC: young controls; CU: elderly cognitively unimpaired; MCI: mildly cognitively impaired; AD: Alzheimer's disease.

SUVr tau positivity cutoff points for each region were calculated using the ROC analysis and Youden's J index, with either (i) amyloid status along with cognitive diagnosis (i.e., A- eCU vs. A+ MCI/AD) or (ii) tau visual read (i.e., visual T+ vs. visual T-) considered as gold standard. In each case, cutoff points were determined as the SUVr value that best separates the two considered groups. Corresponding ROC curves are shown in Figure 20.

Table 5. Tau positivity cutoff points calculated using different analytical methods for different composite regions.

Analytic method \ Composite region	Braak I-II	Braak III-IV	Braak V-VI	Temporal meta-ROI	Early tau
Youden's J index (A- eCU vs. A+ CI)	1.26	1.18	1.17	1.29	1.20
Youden's J index (VR+ vs. VR-)	1.22	1.18	1.11	1.29	1.20
mean+2×SD (A- eCU)	1.34	1.25	1.17	1.30	1.27
mean+2×SD (YC)	1.20	1.22	1.21	1.24	1.24

YC: young controls; eCU: elderly cognitively unimpaired; CI: cognitively impaired (MCI and AD); VR: visual read.

For comparison purposes, tau positivity cut-off points were also calculated as two standard deviations above the mean (*mean+2×SDs*) SUVr of either amyloid-negative (A-) eCU or YC subjects. Note that YC subjects were all amyloid negative.

SUVr value distribution per each composite region are shown in Figure 18, whereas Figure 19 shows average SUVr images corresponding to each of the diagnostic groups considered.

Maximizing Youden's J index determined cutoff points, with amyloid status and clinical diagnosis vs. visual read used as label were Braak I-II (1.26 vs. 1.22), Braak III-IV (1.18 vs. 1.18), Braak V-VI (1.17 vs. 1.11), temporal meta-ROI (1.29 vs. 1.29), and early tau (1.20 vs. 1.20). These cutoff points were determined without including the YC subjects in the ROC analysis.

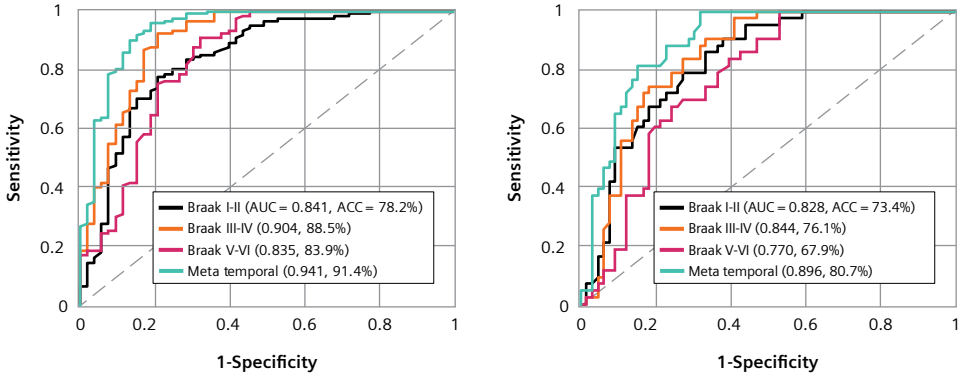

Figure 20. Receiver operating characteristic (ROC) analysis using either (right) amyloid status and cognitive diagnosis (i.e., A- cognitively unimpaired vs. A+ cognitively impaired (MCI/AD)) or (left) positive vs. negative visual read as gold standard. In each case, the SUVr cutoff point was determined as the value that best separates the two considered groups by maximizing Youden's J index. YC subjects were not included. AUC: area under the ROC curve; ACC: accuracy.

Whether using visual read or clinical diagnosis as the gold standard, cutoff points were consistent across all composite regions, except for Braak I-II and for the temporal meta-ROI where the cutoff points decreased from 1.26 to 1.21 and from 1.29 to 1.26, respectively, when including the YC subjects. Table 5 summarizes all cutoff points.

The cutoff point (SUVr = 1.29) for the temporal meta-ROI was consistent across analytical methods and reference populations but, as expected, it was lower (SUVr = 1.24) when taking the *mean+2×SD* of the YC subjects. Note that a YC population is not representative of the typical patient population and hence a cutoff point should not be calculated based only on such a cohort.

Comparison of visual and SUVr-based classifications

SUVr-based classification (using all three temporal meta-ROI cutoff points) compared to visual interpretation led to an overall 90.5% (171/189) concordance rate, as shown on Figure 21. More discordant 'V-/Q+' cases were observed when the cutoff point corresponds to *mean+2×SD* SUVr of the YC cohort (7.9%) was used compared to when using *mean+2×SD* of the A- eCU and when using Youden's index (2.7% and 3.7% discordance, respectively) (see Figure 21).

Intra-class coefficient (ICC), with values raging between 0 (no agreement) and 1 (perfect agreement), was used to compare concordance between the two interpretation methods (rater 1 and rater 2). There was high concordance with ICC = 0.86 ([0.81, 0.90] 95%CI). The *mean+2×SD* threshold of the YC subjects (*SUVr = 1.24*) led to the lowest concordance with visual interpretation with an ICC = 0.84 ([0.80, 0.89] 95%CI).

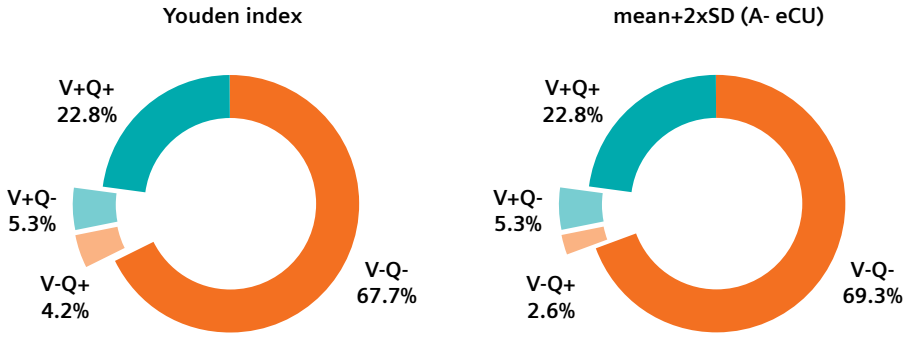

Figure 21. Concordance between visual read (V+/V-) and SUVr-based classification (Q+/Q-) of the A05 cohort (n = 189). Results correspond to using SUVr cutoff points for the temporal meta-region calculated either with ROC analysis and Youden index (left) or using the *mean+2xSD* of the amyloid negative cognitively unimpaired elderly (A-eCU) (right). V: visual; Q: quantitative.

Braak staging with the established T+ thresholds

The Youden's index-based Braak cutoff points calculated using amyloid status and clinical diagnosis as the gold standard were used to hierarchically assign subjects to one of the three Braak stages (Braak I-II, Braak III-IV, or Braak V-VI) or to Braak 0, defined as the stage where SUVr values for all three Braak composite regions are lower than their respective cutoff points. A subject is hierarchically assigned to a Braak stage if they are T+ for that stage and for all lower stages, otherwise, the subject is categorized as Braak-staging discordant. For example, a Braak V-VI subject has all three Braak SUVrs higher than their corresponding cutoff points.

Table 6 summarizes subjects' characteristics classified into different Braak stages, where the first row shows mean ^{18}F-flortaucipir SUVr images for different Braak stages. These images clearly demonstrate ^{18}F-flortaucipir retention progression to the inferior and lateral temporal lobe followed by further progression to other isocortical regions in subsequent Braak stages.

Table 6. Hierarchical Braak staging based on Youden's index cutoff points with clinical diagnosis and amyloid status as labeled.

Average flortaucipir SUVr brain* 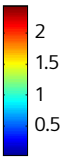	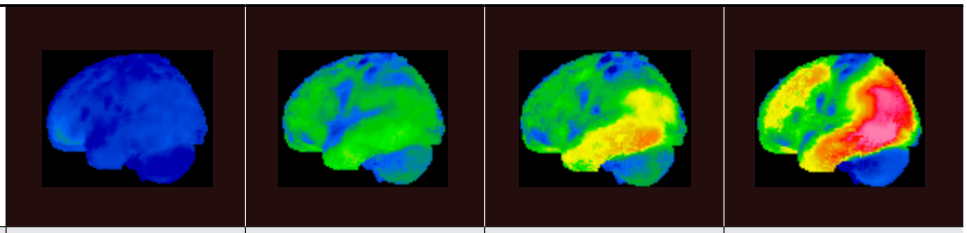			
Braak stage	**Braak 0**	**Braak I-II**	**Braak III-IV**	**Braak V-VI**
N (YC/eCU/MCI/AD)	14/39/49/17	0/6/14/5	0/1/6/3	0/0/12/15
Age	64.38 (16.15)	74.12 (6.95)	79.60 (9.8)	69.81 (9.52)
MMSE	27.8 (3.09)	28.04 (1.54)	24.6 (3.47)	23.19 (5.05)
ADAS Cog-11 score	8.91 (6.32)	9.6 (4.34)	15.1 (5.63)	18.96 (9.27)
% T+ (Visual read)	6.7 (8/119)	28 (7/25)	80 (8/10)	100 (27/27)
% A+ (Visual read)	16.8 (20/119)	44 (11/25)	90 (9/10)	100 (27/27)

*Intensity normalized to mean uptake in inferior cerebellar cortex. YC: young controls; eCU: elderly cognitively unimpaired; MCI: mild cognitively impaired; AD: Alzheimer's disease; MMSE: mini-mental examination score; ADAS cog-11: AD assessment scale–cognitive subscale; T+: tau positive; and A+: amyloid positive.

These results also show that Braak staging is associated with declined cognitive performance as illustrated by the decrease in MMSE score and the increase in ADAS Cog-11 score. Also shown is an increase in amyloid burden as measured with florbetapir SUVR, as well as an increase in the percentage of PET scans (both amyloid and tau) visually interpreted as being positive with advancing Braak stages. All Braak V-VI subjects (100%) had a T+ visual read indicating a perfect agreement between SUVr-based Braak staging and visual read for these higher Braak stages. These subjects were all amyloid positive MCI and AD subjects. Eighty percent (8/10) of Braak III-IV and only 28% (7/25) of Braak I-II had a visual T+ read, indicating a moderate-to-high concordance of hierarchical Braak staging with visual interpretation for the limbic and neocortical stages. Of note also is that only 4.2% (8/189) of all cases were Braak staging discordant.

Independent validation

The validity of the generated tau positivity cutoff points in comparison to visual rating, which is considered as the clinical standard, was also assessed on an independent clinical cohort acquired at *Hôpitaux Universitaires de Geneve* (HUG) (N = 244) with an average age equal to 71 ± 9 years, including healthy controls, MCI and AD patients, as well as a subgroup (N = 11) of patients with other neurodegenerative and psychiatric disorders. Each subject had a ^{18}F-flortaucipir scan, which was visually classified by an expert reader as either tau positive or negative according to the manufacturer's guidelines. ^{18}F-flortaucipir scans were also quantified using *syngo*.MI Neuro Cortical Analysis.

SUVr cutoff points for the temporal meta-ROI were calculated once again on this new cohort and were compared to the ones calculated above on the A05 cohort. When using Youden's index with amyloid status and clinical diagnosis as gold standard, the same cutoff point of 1.29 was obtained using the HUG cohort indicating a reproducible cutoff value with both cohorts. Slight differences in sensitivity and specificity were found though (i.e., Sen: 0.95 vs. 1.00 and Spec: 0.62 vs. 0.61 for HUG vs. A05 cohorts). When visual read was used as gold standard instead, the A05 cut off point was 1.29 (Sen: 0.97, Spec: 0.74) vs. 1.34 (Sen: 0.95, Spec: 0.79) for the HUG cohort. Overall, the cutoff points were all comparable across the two cohorts.

In addition, the temporal meta-ROI cutoff points calculated on the A05 cohort using all analytical methods (Table 5) were used to classify HUG subjects as T+/T- based on their SUVr values, and the corresponding results were compared to visual read using the intra-class correlation coefficient. High concordances between the two classifications were found with ICC ranging from 0.78 to 0.84. The corresponding results are shown in Figure 22.

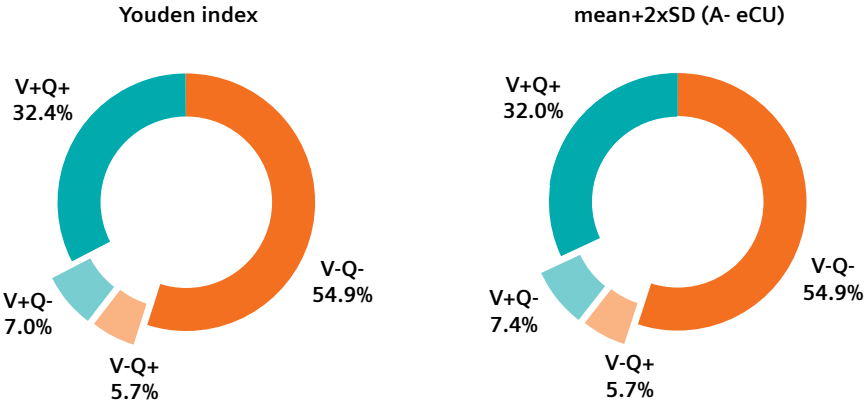

Figure 22. Concordance between visual read (V+/V-) and SUVr-based classification (Q+/Q-) of HUG cohort. Results correspond to using SUVr cutoff points for the temporal meta-region calculated either with ROC analysis and Youden index (left) or using the *mean+2xSD* (right) of the amyloid negative cognitively unimpaired elderly (A- eCU) (see Table 5). V: visual; Q: quantitative.

The future of amyloid and tau PET imaging

According to the National Institute on Aging and Alzheimer's Association (NIA-AA) research framework, known as the AT(N) research framework[57], AD is defined biologically by abnormal levels of biomarkers measuring Aβ and NFTs. Various biomarkers, including CSF and plasma markers, can provide in-vivo measurement of AD proteinopathies. However, PET imaging, of both amyloid and tau, is considered as a reference diagnosis tool. Furthermore, according to the recently published revised criteria for diagnosis and staging of AD[58], amyloid PET is classified as an early changing Core 1 biomarker with sufficient accuracy suitable for early detection of AD in asymptomatic subjects and for confirming AD pathology in symptomatic patients. On the other hand, classified as a later-changing Core 2 biomarker, tau PET is set to play a major prognostic role as it can, when abnormal, increase confidence that symptoms are due to AD.

Combined with amyloid PET, tau PET is also a key marker in the newly proposed biological AD staging.[58] This divides the disease into four different stages based on the magnitude and the topographic information of tau pathology, that can only be captured by PET imaging. For instance, abnormal amyloid deposition with tau PET aggregates restricted to the medial temporal areas (i.e., A+/T_{MTL+}) constitutes a stage (Stage B) different than the advanced stages C and D that are defined with the presence of abnormal amyloid and moderate-to-high neocortical tau burden, respectively, as measured with SUVr (i.e., A+/T_{NEO+} and A+/T_{NEO++}). Stage A, known as the initial biological stage, is defined by abnormal amyloid PET with no uptake on tau PET (A+/T-). Note that a similar fluid-only staging scheme can be considered, but such a scheme can only be regarded as conceptual at present, as more fluid biomarkers that are closely correlated with tau PET are being developed.[58]

Two large, multi-site studies have assessed the clinical utility of amyloid PET, the IDEAS and AMYPAD studies, which show that using amyloid PET changes both diagnosis and patient management, and improves timely diagnostic workup of memory clinic patients. In addition, it was shown that amyloid PET quantification can be used to accurately predict cognitive decline.[59]

Visually interpreting amyloid PET scans remains the standard approach, but quantification helps resolve borderline and ambiguous cases by enhancing visual assessments, especially for less experienced readers. The EU and UK updated the labels of approved amyloid PET radiotracers to include quantification as an adjunct to visual assessment. Amyloid PET quantification with the tracer-independent CL scale is instrumental in designing anti-amyloid drug trials and in assessing treatment efficacy. CL-based quantification of amyloid PET scans will play a major role in guiding clinical management decisions of patients under treatment through precise monitoring of amyloid clearance in the brain.

On the other hand, the clinical utility of tau PET was recently highlighted in a prospective study (N = 878)[60], which showed that including tau PET in the diagnostic workup was associated with a significant change in diagnosis and an increase in diagnostic certainty. Tau PET was also associated with a significant change in patient treatment and management. The clinical utility of tau PET has also been shown in a recent anti-amyloid drug trial for participant selection and as the trial secondary end point to assess the drug effect on tau pathology.[61]

In another anti-amyloid drug trial, recent results showed that cognitive benefits are greater when the treatment is started at earlier disease stages (i.e., no or low tau as measured with PET) and that these benefits could be maintained over three years of treatment.[62]

Given the close correlation of tau with disease severity in AD, and the presence of tau pathology in other non-AD tauopathies, several tau-targeted drugs are being developed.[63] Tau biomarkers, including tau PET, are set to play a major role in these trials for patient selection, assessment of drug efficacy and study outcome, and have the potential to accelerate the success of these trials.

Finally, with the advent of tau PET ligands and the development of ligands that bind preferentially to specific tauopathies other than the mixed 3R/4R AD tauopathy, tau PET imaging is a promising tool for the differential diagnosis of different tauopathies[5] and in the work-up of AD phenotypes[8] where ^{18}F-flortaucipir uptake patterns were shown to match the different clinical and the neuroanatomical presentations of typical and atypical AD phenotypes.

Conclusion

This white paper describes quantification methods used for amyloid and tau PET in *syngo*.MI Neuro Cortical Analysis. The methods have been developed so as not to require an MRI for processing. They rely on transforming the input patient scan into the MNI standard space prior to calculating SUVr values on predefined anatomical volumes of interest. The spatial normalization to MNI space is based on a novel PET-to-PET deformable registration approach, which was first developed for amyloid PET scans and was extended to ^{18}F-flortaucipir PET images. Several validation experiments were performed to assess the performance of the implemented quantification methods against visual read as well as against other (MRI-based) quantification approaches.

Validation was carried out for the three commercially available amyloid radiotracers (florbetapir, florbetaben, and flutemetamol) and for the only FDA approved tau tracer, ^{18}F-flortaucipir. Efforts to extend these methods to next generation amyloid (e.g., ^{18}F-NAV-4694) and tau tracers (e.g., ^{18}F-PI-2620 and ^{18}F-MK-6240) are ongoing.

To help interpret quantification results and to allow Braak staging, SUVr-based tau positivity thresholds were established using data from a trial cohort and were further validated on an independent memory clinic cohort. The established cutoff points compare favorably to values previously published by other groups. Users can use their own imaging data to determine site and population-specific cutoff points for specific clinical questions. The introduced ^{18}F-flortaucipir quantification solution might need to be updated to support second generation tau tracers and to potentially be used in non-AD tauopathies, due to the differences between tau tracers in binding characteristics and off target sites. This may involve, for instance, using different ROIs for SUVr calculation, modification of the existing PET-to-PET registration to MNI space, and eventually defining tracer-specific abnormality thresholds.

Differences in binding characteristics between tau PET radiotracers could make it challenging to compare outcomes across tracers, demonstrating a potential need for a harmonization method such as the *CenTauR* method[64-65]. Finally, even though the temporal meta-ROI yields high discriminatory accuracy between AD and non-AD neurodegenerative conditions[49], other ROIs might be more suitable for differential diagnosis of atypical tauopathies and AD phenotypes.

About the authors

Rachid Fahmi, PhD, received a MSc and a doctorate degree in applied mathematics from University of Metz, France, and then completed a PhD in electrical and computer engineering at the University of Louisville, Kentucky, USA, in 2008. He has worked in medical imaging since 2003 both at the University of Louisville, and at Case Western Reserve University in Cleveland, Ohio, USA. He is currently a senior staff scientist within the research and clinical collaborations team of Siemens Healthineers Molecular Imaging, which he first joined in the summer of 2015. Since then, he has been leading the scientific development of software solutions for molecular imaging applications in neurology.

Günther Platsch, MD, studied medicine at the University of Erlangen-Nuremberg since 1982 and passed the final exams in 1988. From 1988 to 2004, he worked as an assistant physician, and later as a senior physician at the department of Nuclear Medicine at the University of Erlangen-Nuremberg. He received a Doctorate degree in Medicine in 1991 (Dr. med.) and became a board-certified Nuclear Medicine Physician in 1992. In 2004, Günther Platsch joined Siemens AG as a clinical scientist in Siemens Molecular Imaging, and since 2011 as a Senior Key Expert. In this position, he provides medical input for clinical application development as well as in SPECT and PET development.

References

[1] **Odero-Tavoletti MT, Rowe CC, McLean CA, et al.** Characterization of PiB binding to white matter in Alzheimer disease and other dementias. *J Nucl Med.* 2009;50(2):198-204.

[2] **Klunk WE, Koeppe RA, Price JC, et al.** The Centiloid Project: standardizing quantitative amyloid plaque estimation by PET. *Alzheimer's Dement.* 2015;11(1):1-15.e154. doi:10.1016/j.jalz.2014.07.003.

[3] **Rabinovici GD, Gatsonis C, Apgar C, et al.** Association of Amyloid Positron Emission Tomography with Subsequent Change in Clinical Management Among Medicare Beneficiaries with Mild Cognitive Impairment or Dementia. *JAMA.* 2019;321(13):1286-1294.

[4] **Altomare D, Barkhof F, Caprioglio C, et al.** Clinical Effect of Early vs Late Amyloid Positron Emission Tomography in Memory Clinic Patients: The AMYPAD-DPMS Randomized Clinical Trial. *JAMA Neurol.* 2023;80(6):548-557.

[5] **Leuzy A, Chiotis K, Lemoine L, et al.** Tau PET imaging in neurodegenerative tauopathies-still a challenge. *Mol Psychiatry.* 2019;24(8):1112-1134.

[6] **Messerschmidt K, Barthel H, Brendel M, et al.** ^{18}F-PI-2620 Tau PET Improves the Imaging Diagnosis of Progressive Supranuclear Palsy. *J Nucl Med.* 2022;63(11):1754-1760. doi:10.2967/jnumed.121.262854.

[7] **Laccarino L, La Joie R, Edwards L, et al.** Spatial Relationships between Molecular Pathology and Neurodegeneration in the Alzheimer's Disease Continuum. *Cereb Cortex.* 2021;31(1):1-14. doi:10.1093/cercor/bhaa184.

[8] **Ossenkoppele R, Schonhaut DR, Schöll M, et al.** Tau PET patterns mirror clinical and neuroanatomical variability in Alzheimer's disease. *Brain.* 2016;139(Pt 5):1551-1567. doi:10.1093/brain/aww027.

[9] **La Joie R, Visani AV, Baker SL, et al.** Prospective longitudinal atrophy in Alzheimer's disease correlates with the intensity and topography of baseline tau-PET. *Sci Transl Med.* 2020;12(524):eaau5732. doi:10.1126/scitranslmed.aau5732.

[10] **Ossenkoppele R, Smith R, Mattsson-Carlgren N, et al.** Accuracy of Tau Positron Emission Tomography as a Prognostic Marker in Preclinical and Prodromal Alzheimer Disease: A Head-to-Head Comparison Against Amyloid Positron Emission Tomography and Magnetic Resonance Imaging. *JAMA Neurol.* 2021;78(8):961-971. doi:10.1001/jamaneurol.2021.

[11] **Costoya-Sánchez A, Moscoso A, Silva-Rodríguez J, et al.** Increased Medial Temporal Tau Positron Emission Tomography Uptake in the Absence of Amyloid-β Positivity. *JAMA Neurol.* 2023;80(10):1051-1061. doi:10.1001/jamaneurol.2023.2560.

[12] **Braak H, Braak E.** Neuropathological stageing of Alzheimer-related changes. *Acta Neuropathol.* 1991;82(4):239-259. doi:10.1007/BF00308809.

[13] **Braak H, Alafuzoff I, Arzberger T, Kretzschmar H, Del Tredici K.** Staging of Alzheimer disease-associated neurofibrillary pathology using paraffin sections and immunocytochemistry. *Acta Neuropathol.* 2006;112(4):389-404. doi:10.1007/s00401-006-0127-z.

[14] **Braak H, Thal DR, Ghebremedhin E, Del Tredici K.** Stages of the pathologic process in Alzheimer disease: age categories from 1 to 100 years. *J Neuropathol Exp Neurol.* 2011;70(11):960-969. doi:10.1097/NEN.

[15] **Marquié M, Siao Tick Chong M, Antón-Fernández A, et al.** [F-18]-AV-1451 binding correlates with postmortem neurofibrillary tangle Braak staging. *Acta Neuropathol.* 2017;134(4):619-628. doi:10.1007/s00401-017-1740-.

[16] **Schwarz AJ, Yu P, Miller BB, et al.** Regional profiles of the candidate tau PET ligand ^{18}F-AV-1451 recapitulate key features of Braak histopathological stages. *Brain.* 2016;139(Pt 5):1539-1550. doi:10.1093/brain/.

[17] **Cho H, Choi JY, Hwang MS, et al.** In vivo cortical spreading pattern of tau and amyloid in the Alzheimer disease spectrum. *Ann Neurol.* 2016;80(2):247-258. doi:10.1002/ana.

[18] **Schöll M, Lockhart SN, Schonhaut DR, et al.** PET Imaging of Tau Deposition in the Aging Human Brain. *Neuron.* 2016;89(5):971-982. doi:10.1016/j.neuron.2016.01.

[19] **Goedert M, Falcon B, Clavaguera F, Tolnay M.** Prion-like mechanisms in the pathogenesis of tauopathies and synucleinopathies. *Curr Neurol Neurosci Rep.* 2014;14(11):495. doi:10.1007/s11910-014-0495-z.

[20] **Lowe VJ, Wiste HJ, Senjem ML, et al.** Widespread brain tau and its association with ageing, Braak stage and Alzheimer's dementia. *Brain.* 2018;141(1):271-287. doi:10.1093/brain/awx320.

[21] **Vogel JW, Young AL, Oxtoby NP, et al.** Four distinct trajectories of tau deposition identified in Alzheimer's disease. *Nat Med.* 2021;27(5):871-881. doi:10.1038/s41591-021-01309-.

[22] **Jean-Marc Peyrat, Abhinay Joshi, Mark Mintun et al.** An automatic method for the quantification of uptake with Florbetapir imaging. *J Nucl Med.* 2012;53 (Supplement 1):210.

[23] **Fleisher AS, Chen K, Liu X, et al.** Using positron emission tomography and florbetapir F18 to image cortical amyloid in patients with mild cognitive impairment or dementia due to Alzheimer disease. *Arch Neurol.* 2011;68(11):1404-1411.

[24] **Tzourio-Mazoyer N, Landeau B, Papathanassiou D, et al.** Automated anatomical labeling of activations in SPM using a macroscopic anatomical parcellation of the MNI MRI single-subject brain. *Neuroimage.* 2002;15(1):273-289. doi:10.1006/nimg.2001.0978.

[25] **Barthel H, Gertz HJ, Dresel S, et al.** Cerebral amyloid-β PET with florbetaben (18F) in patients with Alzheimer's disease and healthy controls: a multicentre phase 2 diagnostic study. *Lancet Neurol.* 2011;10(5):424-435.

[26] **Hutton C, Declerck J, Mintun MA, et al.** Quantification of ^{18}F-florbetapir PET: comparison of two analysis methods. *Eur J Nucl Med Mol Imaging.* 2015;42(5): 725-732.

[27] **Hutton C, Sibille L, Bullich S.** Comparison of two methods, with and without MRI, for quantification of florbetaben (18F) PET. EANM'14. *Eur J Nucl Med Mol Imaging* 41 (Suppl 2), 151–705 (2014).

[28] **Hutton C, Sibille L, Thomas B, et al.** Quantification of ^{18}F-flutemetamol PET: Comparison of purely PET with MR and PET based methods. EANM'14. *Eur J Nucl Med Mol Imaging* 41 (Suppl 2), 151–705 (2014).

[29] **Joshi AD, Pontecorvo MJ, Clark CM, et al.** Performance characteristics of amyloid PET with florbetapir F 18 in patients with Alzheimer's disease and cognitively normal subjects. *J Nucl Med.* 2012;53(3):378-384.

[30] **Lundqvist R, Lilja J, Thomas BA, et al.** Implementation and validation of an adaptive template registration method for ^{18}F-flutemetamol imaging data. *J Nucl Med.* 2013;54(8):1472-1478.

[31] Alzheimer's Disease Neuroimaging Initiative (ADNI): https://adni.loni.usc.edu/.

[32] **Thurfjell L, Lilja J, Lundqvist R, et al.** Automated quantification of ^{18}F-flutemetamol PET activity for categorizing scans as negative or positive for brain amyloid: concordance with visual image reads. *J Nucl Med.* 2014;55(10):1623-1628.

[33] **Sibille L, Hutton C, and Declerck J.** Deformable registration for ^{18}F-florbetapir PET quantification. *Eur J Nucl Med Mol Imaging* 42, S575-S575 (2015).

[34] Statistical Parametric Mapping (SPM): https://www.fil.ion.ucl.ac.uk/spm/.

[35] The Global Alzheimer's Association Interactive Network (GAAIN): https://www.gaain.org/centiloid-project.

[36] **Rachid Fahmi.**, "Centiloid Calibration of a Commercial Amyloid Quantitation Software for different Fluorine-18 Radiotracers". European Association of Nuclear Medicine (EANM) conference 2023, Vienna, Austria, September 9-13, 2023.

[37] **Hirschmüller K, Prieto E, Mínguez F, et al.** Visual Reading and Centiloid Scaling for the Evaluation of Brain Amyloid PET Imaging in Patients with Mild Cognitive Impairment: Impact on Conversion to Alzheimer's Disease Dementia. European Association of Nuclear Medicine (EANM) conference 2024, Hamburg, Germany, October 19-23, 2024.

[38] **De Souza GS, Andrade MA, Borelli WV, et al.** Amyloid-β PET Classification on Cognitive Aging Stages Using the Centiloid Scale. *Mol Imaging Biol.* 2022;24(3):394-403. doi:10.1007/s11307-021-01660-7.

[39] **Collij LE, Bollack A, La Joie R, et al.** Centiloid recommendations for clinical context-of-use from the AMYPAD consortium. *Alzheimers Dement.* 2024;20(12):9037-9048. doi:10.1002/alz.14336.

[40] **Ruwanpathirana GP, Williams RC, Masters CL, et al.** Impact of PET Reconstruction on Amyloid-β Quantitation in Cross-Sectional and Longitudinal Analyses. *J Nucl Med.* 2024 May 1;65(5):781-787. doi: 10.2967/jnumed.123.266188.

[41] **Zhang J, Soleimani-Meigooni DN, Koeppe R, et al.** Exploring Centiloid Robustness: Impact of Sample Size and Image Resolution on Centiloid Conversion Accuracy. *J Nucl Med.* 2025 Dec 3;66(12):1976-1984. doi: 10.2967/jnumed.125.270607.

[42] **Shekari M, Vállez García D, Collij LE, et al.** Stress testing the Centiloid: Precision and variability of PET quantification of amyloid pathology. *Alzheimers Dement.* 2024;20(8):5102-5113. doi:10.1002/alz.13883.

[43] **Fleisher AS, Pontecorvo MJ, Devous MD Sr, et al.** Positron Emission Tomography Imaging with [18F]flortaucipir and Postmortem Assessment of Alzheimer Disease Neuropathologic Changes [published correction appears in *JAMA Neurol.* 2023 Aug 1;80(8):873.

[44] Label for ^{18}F-flortaucipir: https://www.accessdata.fda.gov/drugsatfda_docs/label/2020/212123s000lbl.pdf

[45] **Sims JR, Zimmer JA, Evans CD, et al.** Donanemab in Early Symptomatic Alzheimer Disease: The TRAILBLAZER-ALZ 2 Randomized Clinical Trial. *JAMA.* 2023;330(6):512-527. doi:10.1001/jama.2023.13239.

[46] **Pontecorvo MJ, Devous MD Sr, Navitsky M, et al.** Relationships between flortaucipir PET tau binding and amyloid burden, clinical diagnosis, age and cognition. *Brain.* 2017;140(3):748-763. doi:10.1093/brain/aww334.

[47] **Baker SL, Maass A, Jagust WJ.** Considerations and code for partial volume correcting [18F]-AV-1451 tau PET data. *Data Brief.* 2017;15:648-657. Published 2017 Oct 16. doi:10.1016/j.dib.2017.10.024.

[48] **Landau S, Korman D, and Jagust W.** Flortaucipir (AV-1451) processing methods. Available online: https://ida.loni.usc.edu/.

[49] **Jack CR Jr, Wiste HJ, Weigand SD, et al.** Defining imaging biomarker cut points for brain aging and Alzheimer's disease. *Alzheimers Dement.* 2017;13(3):205-216. doi:10.1016/j.jalz.2016.08.005.

[50] **Ossenkoppele R, Rabinovici GD, Smith R, et al.** Discriminative Accuracy of [18F]flortaucipir Positron Emission Tomography for Alzheimer Disease vs Other Neurodegenerative Disorders. *JAMA.* 2018;320(11):1151-1162. doi:10.1001/jama.2018.12917.

[51] **Kotari V, Southekal S, Navitsky M, et al.** Early tau detection in flortaucipir images: validation in autopsy-confirmed data and implications for disease progression. *Alzheimers Res Ther.* 2023;15(1):41. Published 2023 Feb 28. doi:10.1186/s13195-023-01160-6.

[52] **Fahmi R.** A PET only F-18-flortaucipir quantification: comparison with an MRI-based method. *European Journal of Nuclear Medicine And Molecular Imaging.* Vol. 48. No. SUPPL 1. S172-S172.

[53] **Weigand AJ, Maass A, Eglit GL, Bondi MW.** What's the cut-point?: a systematic investigation of tau PET thresholding methods. *Alzheimers Res Ther.* 2022;14(1):49. Published 2022 Apr 5. doi:10.1186/s13195-022-00986-w.

[54] **Villemagne VL, Lopresti BJ, Doré V, et al.** What Is T+? A Gordian Knot of Tracers, Thresholds, and Topographies. *J Nucl Med.* 2021;62(5):614-619. doi:10.2967/jnumed.120.245423.

[55] **Maass A, Landau S, Baker SL, et al.** Comparison of multiple tau-PET measures as biomarkers in aging and Alzheimer's disease. *Neuroimage.* 2017;157:448-463. doi:10.1016/j.neuroimage.2017.05.058.

[56] **Chen CD, Ponisio MR, Lang JA, et al.** Comparing Tau PET Visual Interpretation with Tau PET Quantification, Cerebrospinal Fluid Biomarkers, and Longitudinal Clinical Assessment. *J Alzheimers Dis.* 2023;93(2):765-777. doi:10.3233/JAD-230032.

[57] **Jack CR Jr, Bennett DA, Blennow K, et al.** NIA-AA Research Framework: Toward a biological definition of Alzheimer's disease. *Alzheimers Dement.* 2018;14(4):535-562. doi:10.1016/j.jalz.2018.02.018.

[58] **Jack CR Jr, Andrews JS, Beach TG, et al.** Revised criteria for diagnosis and staging of Alzheimer's disease: Alzheimer's Association Workgroup. *Alzheimers Dement.* 2024;20(8):5143-5169. doi:10.1002/alz.13859.

[59] **Hanseeuw BJ, Malotaux V, Dricot L, et al**. Defining a Centiloid scale threshold predicting long-term progression to dementia in patients attending the memory clinic: an [18F] flutemetamol amyloid PET study. *Eur J Nucl Med Mol Imaging.* 2021;48(1):302-310. doi:10.1007/s00259-020-04942-4.

[60] **Smith R, Hägerström D, Pawlik D, et al.** Clinical Utility of Tau Positron Emission Tomography in the Diagnostic Workup of Patients with Cognitive Symptoms. *JAMA Neurol.* 2023;80(7):749-756. doi:10.1001/jamaneurol.2023.1323.

[61] **Mintun MA, Lo AC, Duggan Evans C, et al.** Donanemab in Early Alzheimer's Disease. *N Engl J Med.* 2021;384(18):1691-1704. doi:10.1056/NEJMoa2100708.

[62] **Selkoe DJ, Dhadda S, Irizarry MC, Kramer LD.** Does the Current Evidence for Lecanemab Mechanism Support a Rationale for Continued Lecanemab Dosing?. *Alzheimers Dement.* 2025;20(Suppl 6):e092090. Published 2025 Jan 9. doi:10.1002/alz.092090.

[63] **Cummings JL, Gonzalez MI, Pritchard MC, May PC, Toledo-Sherman LM, Harris GA.** The therapeutic landscape of tauopathies: challenges and prospects. *Alzheimers Res Ther.* 2023;15(1):168. Published 2023 Oct 6. doi:10.1186/s13195-023-01321-7.

[64] **Leuzy A, Raket LL, Villemagne VL, et al.** Harmonizing tau positron emission tomography in Alzheimer's disease: The CenTauR scale and the joint propagation model. *Alzheimers Dement* 2024; 20:5833-5848

[65] **Villemagne VL, Leuzy A, Bohorquez SS, et al.** CenTauR: Toward a universal scale and masks for standardizing tau imaging studies. *Alzheimers Dement (Amst).* 2023;15(3):e12454. Published 2023 Jul 7. doi:10.1002/dad2.12454.

Siemens Healthineers Headquarters
Siemens Healthineers AG
Siemensstr. 3
91301 Forchheim
Germany
Phone: +49 9191 18-0
siemens-healthineers.com

Published by
Siemens Medical Solutions USA, Inc.
2501 N. Barrington Road
Hoffman Estates, IL 60192
USA
Phone: +1 847 304-7700
siemens-healthineers.com/mi